

# Geochemical inverse modeling of chemical and isotopic data from groundwaters in Sahara (Ouargla basin, Algeria)

R. Slimani<sup>a</sup>, A. Guendouz<sup>b</sup>, F. Trolard<sup>c</sup>, A.S. Moulla<sup>d</sup>, B. Hamdi-Aïssa<sup>a</sup>, G. Bourrié<sup>c</sup>

<sup>a</sup>*Ouargla Univ., Fac. des Sciences de la Nature et de la Vie, Lab. Biochimie des Milieux Désertiques, Ouargla 30000, Algeria*

<sup>b</sup>*Blida University, Science and Engineering Faculty, P.O.Box 270 Soumaa, Blida, Algeria*

<sup>c</sup>*INRA, UMR 1114 Emmah, Avignon, France*

<sup>d</sup>*Algiers Nuclear Research Centre, P.O. Box, 399 Alger-RP, 16000 Algiers, Algeria*

## Abstract

Unpublished chemical and isotopic data taken in November 1992 from the three major Saharan aquifers namely, the “Continental Intercalaire” (CI), the “Complexe Terminal” (CT) and the Phreatic aquifer (Phr) were integrated with original samples in order to chemically and isotopically characterize a Saharan aquifer system and investigate the processes through which groundwaters acquire their mineralization. Instead of classical Debye-Hückel extended law, Specific Interaction Theory (SIT) model, recently incorporated in Phreeqc 3.0 was used. Inverse modeling of hydrochemical data constrained by isotopic data was used here to quantitatively assess the influence of geochemical processes: at depth, the dissolution of salts from the geological formations during upward leakage without evaporation explains the transitions from CI to CT and to a first end member, cluster of Phr (cluster I); near the surface, the dissolution of salts from sebkhas by rainwater explains another cluster of Phr (cluster II). In every case, secondary precipitation of calcite occurs during dissolution. All Phr waters result from the mixing of these two clusters together with calcite precipitation and ion exchange processes. These processes are quantitatively assessed by Phreeqc model. Globally, gypsum dissolution and calcite precipitation were found to act as a carbon sink.

**Keywords:** hydrochemistry, stable isotopes, Sahara, Algeria

## 1. INTRODUCTION

A scientific study published in 2008 (OECD, 2008) showed that 85% of the world population lives in the driest half of the Earth. More than 1 billion people residing in arid and semi-arid areas of the world have only access to little or no renewable water resources. In many arid regions such as Sahara, groundwater is the only source of water supply for domestic, agricultural or industrial purposes, often causing overuse and / or degradation of water quality.

The groundwater resources of Ouargla basin (Lower-Sahara, Algerian) (Fig. 1) are contained in three main reservoirs (UNESCO, 1972; Eckstein and Eckstein, 2003; OSS, 2003, 2008):

---

*Email address:* slm\_rabia@yahoo.fr (R. Slimani)

- 19 • at the top, the phreatic aquifer (Phr), located in sandy gypsum permeable formations of  
20 Quaternary, is almost unexploited, due to its salinity (50 g/L);
- 21 • in the middle, the “Complexe Terminal” (CT) (Cornet and Gouscov, 1952; UNESCO,  
22 1972) is the most exploited and includes several aquifers in different geological forma-  
23 tions. Groundwater circulates in one or two lithostratigraphic formations of the Eocene  
24 and Senonian carbonates or Mio-pliocene sands;
- 25 • at the bottom, the “Continental Intercalaire” (CI), hosted in the lower Cretaceous continen-  
26 tal formations (Barremian and Albian), mainly composed of sandstones, sands and clays.  
27 It is only partially exploited because of its significant depth.

28 After use, waters are discharged in a closed system (endorheic basin) and constitute a po-  
29 tential hazard to the environment, to public health and may jeopardize the sustainability of agri-  
30 culture, due to rising of the phreatic aquifer watertable, extension of soil salinization and so  
31 on (Hamdi-Aïssa et al., 2004; Slimani, 2006). Several studies (Guendouz, 1985; Fontes et al.,  
32 1986; Guendouz and Moulla, 1996; Edmunds et al., 2003; Guendouz et al., 2003; Hamdi-Aïssa  
33 et al., 2004; Foster et al., 2006; OSS, 2008; Al-Gamal, 2011) started from chemical and isotopic  
34 information ( $^2\text{H}$ ,  $^{18}\text{O}$ ,  $^{234}\text{U}$ ,  $^{238}\text{U}$ ,  $^{36}\text{Cl}$ ) to characterize the relationships between aquifers. In  
35 particular, such studies focused on the recharge of the deep CI aquifer system. These investi-  
36 gations dealt particularly with water chemical facies, mapped isocontents of various parameters,  
37 and reported typical geochemical ratios ( $[\text{SO}_4^{2-}]/[\text{Cl}^-]$ ,  $[\text{Mg}^{2+}]/[\text{Ca}^{2+}]$ ) as well as other correla-  
38 tions. Minerals / solutions equilibria were checked by computing saturation indices with respect  
39 to calcite, gypsum, anhydrite and halite, but processes were only qualitatively assessed.

40 The present study aims at applying for the first time ever in Algeria, a new methodology  
41 (inverse modeling) to an extreme environment where lack of data on a scarce natural resource  
42 (groundwater) is observed. New data were hence collected in order to characterize the hydro-  
43 chemical and the isotopic composition of the major aquifers in the Saharan region of Ouargla.  
44 New possibilities offered by progress in geochemical modeling were used. The objective was  
45 also to identify the origin of the mineralization and the water-rock interactions that occur along  
46 the flow. More specifically, inverse modeling of chemical reactions allows one to select the best  
47 conceptual model for the interpretation of the geochemical evolution of Ouargla aquifer system.  
48 The stepwise inversion strategy involves designing a list of scenarios (hypotheses) that take into  
49 consideration the most plausible combinations of geochemical processes that may occur within  
50 the studied medium. After resolving the scenarios in a stepwise manner, the one that provides  
51 the best conceptual geochemical model is then selected (Dai et al., 2006). Inverse modeling  
52 with Phreeqc 3.0 was used to quantitatively assess the influence of the processes that explain  
53 the acquisition of solutes for the different aquifers: dissolution, precipitation, mixing and ion  
54 exchange. This results in constraints on mass balances as well as on the exchange of matter  
55 between aquifers.

## 56 2. METHODOLOGY

### 57 2.1. Presentation of the study area

58 The study area is located in the northeastern desert of Algeria “Lower-Sahara” (Le Houérou,  
59 2009) near the city of Ouargla (Fig. 1),  $31^\circ 54'$  to  $32^\circ 1'$  N and  $5^\circ 15'$  to  $5^\circ 27'$  E, with a mean ele-  
60 vation of 134 (m.a.s.l.). It is located in the quaternary valley of Oued Mya basin. Present climate

61 belongs to the arid Mediterranean-type (Dubief, 1963; Le Houérou, 2009; ONM, 1975/2013), as  
62 it is characterized by a mean annual temperature of 22.5 °C, a yearly rainfall of 43.6 mm/yr and  
63 a very high evaporation rate of 2,138 mm/yr.

64  
65 Ouargla's region and the entire Lower Sahara has experienced during its long geological  
66 history alternating marine and continental sedimentation phases. During Secondary era, vertical  
67 movements affected the Precambrian basement causing in particular collapse of its central part,  
68 along an axis passing approximately through the Oued Righ valley and the upper portion of the  
69 valley oued Mya. According to Furon (1960), a epicontinental sea spread to the Lower Eocene of  
70 northern Sahara. After the Oligocene, the sea gradually withdrew. It is estimated at present that  
71 this sea did not reach Ouargla and transgression stopped at the edge of the bowl (Furon, 1960;  
72 Lelièvre, 1969). The basin is carved into Mio-pliocene (MP) deposits, which alternate with red  
73 sands, clays and sometimes marls; gypsum is not abundant and dated from Pontian (MP) (Cornet  
74 and Gouscov, 1952; Dubief, 1953; Ould Baba Sy and Besbes, 2006). The continental Pliocene  
75 consists of a local limestone crust with puddingstone or lacustrine limestone (Fig. 2), shaped  
76 by eolian erosion into flat areas (regs). The Quaternary formations are lithologically composed  
77 of alternating layers of permeable sand and relatively impermeable marl (Aumassip et al., 1972;  
78 Chellat et al., 2014).

79 The exploitation of Mio-pliocene aquifer is ancient and at the origin of the creation of the  
80 oasis (Lelièvre, 1969; Moulias, 1927). The piezometric level was higher (145 m a.s.l.) but over-  
81 exploitation at the end of the XIXth century led to a catastrophic decrease of the resource, with  
82 presently more than 900 boreholes (ANRH, 2011).

83 The exploitation of Senonian aquifer dates back to 1953 at a depth 140 m to 200 m depth,  
84 with a small initial rate *ca.* 9 L s<sup>-1</sup>; two boreholes have been exploited since 1965 and 1969, with  
85 a total flowrate *ca.* 42 L s<sup>-1</sup>, for drinking water and irrigation.

86 The exploitation of Albian aquifer dates back to 1956, presently, two boreholes are exploited:

- 87 • El Hedeb I, 1,335 m deep, with a flowrate 141 L s<sup>-1</sup>;
- 88 • El Hedeb II, 1,400 m deep, with a flowrate 68 L s<sup>-1</sup>.

## 89 2.2. *Sampling and analytical methods*

90 The sampling programme consisted of collecting samples along transects corresponding to  
91 directions of flow for both Phr and CT aquifers while it was possible to collect only eight samples  
92 from the CI. A total of ( $n = 107$ ) samples were collected during a field campaign in 2013, along  
93 the main flowpath of Oued Mya. 67 of them were from piezometers tapping the phreatic aquifer,  
94 32 from CT wells and the last 8 from boreholes tapping the CI aquifer (Fig. 3). Analyses of  
95 Na<sup>+</sup>, K<sup>+</sup>, Ca<sup>2+</sup>, Mg<sup>2+</sup>, Cl<sup>-</sup>, SO<sub>4</sub><sup>2-</sup> and HCO<sub>3</sub><sup>-</sup> were performed by ion chromatography at Algiers  
96 Nuclear Research Center (CRNA). Previous and yet unpublished data (Guendouz and Moulla,  
97 1996) sampled in 1992 are used here too: 59 samples for Phr aquifer, 15 samples for CT aquifer  
98 and 3 samples for the CI aquifer for chemical analyses, data <sup>18</sup>O and <sup>3</sup>H (Guendouz and Moulla,  
99 1996).

## 100 2.3. *Geochemical method*

101 Phreeqc was used to check minerals / solution equilibria using the specific interaction the-  
102 ory (SIT), *i.e.* the extension of Debye-Hückel law by Scatchard and Guggenheim incorporated  
103 recently in Phreeqc 3.0 (Parkhurst and Appelo, 2013). Inverse modeling was used to calculate

104 the number of minerals and gases' moles that must respectively dissolve or precipitate/degas to  
105 account for the difference in composition between initial and final water end members (Plum-  
106 mer and Back, 1980; Kenoyer and Bowser, 1992; Deutsch, 1997; Plummer and Sprinckle, 2001;  
107 Güler and Thyne, 2004; Parkhurst and Appelo, 2013). This mass balance technique has been  
108 used to quantify reactions controlling water chemistry along flow paths (Thomas et al., 1989).  
109 It is also used to quantify the mixing proportions of end-member components in a flow system  
110 (Kuells et al., 2000; Belkhiri et al., 2010, 2012).

111 Inverse modeling involves designing a list of scenarios (modelling setups) that take into ac-  
112 count the most plausible combinations of geochemical processes that are likely to occur in our  
113 system. For example, the way to identify whether calcite dissolution/precipitation is relevant or  
114 not consists of solving the inverse problem under two alternate scenarios: (1) considering a geo-  
115 chemical system in which calcite is present, and (2) considering a geochemical system without  
116 calcite. After simulating the two scenarios, it is usually possible to select the setup that gives the  
117 best results as the solution to the inverse modeling according to the fit between the modeled and  
118 observed values. Then one can conclude whether calcite dissolution/precipitation is relevant or  
119 not. This stepwise strategy allows us to identify the relevance of a given chemical process by  
120 inversely solving the problem through alternate scenarios in which the process is either partici-  
121 pating or not.

### 122 3. RESULTS AND DISCUSSION

123 Tables 1 to 5 illustrate the results of the chemical and the isotopic analyses. Samples are  
124 ordered according to an increasing electric conductivity (EC), and this is assumed to provide  
125 an ordering for increasing salt content. In both phreatic and CT aquifers, temperature is close to  
126 25 °C, while for CI aquifer, temperature is close to 50 °C. The values presented in tables 1 to 5 are  
127 raw analytical data that were corrected for defects of charge balance before computing activities  
128 with Phreeqc. As analytical errors could not be ascribed to a specific analyte, the correction was  
129 made proportionally. The corrections do not affect the anions to anions mole ratios such as for  
130  $[\text{HCO}_3^-]/([\text{Cl}^-] + 2[\text{SO}_4^{2-}])$  or  $[\text{SO}_4^{2-}]/[\text{Cl}^-]$ , whereas they affect the cation to anion ratio such  
131 as for  $[\text{Na}^+]/[\text{Cl}^-]$ .

#### 132 3.1. *Characterization of chemical facies of the groundwater*

133 Piper diagrams drawn for the studied groundwaters (Fig. 4) broadly show a scatter plot domi-  
134 nated by a Chloride-Sodium facies. However, when going into small details, the widespread  
135 chemical facies of the Phr aquifer is closer to the NaCl cluster than those of CI and CT aquifers.  
136 Respectively,  $\text{CaSO}_4$ ,  $\text{Na}_2\text{SO}_4$ ,  $\text{MgSO}_4$  and NaCl are the most dominant chemical species (min-  
137 erals) that are present in the phreatic waters. This sequential order of solutes is comparable to  
138 that of other groundwater occurring in North Africa, and especially in the neighboring area of  
139 the chotts (depressions where salts concentrate by evaporation) Merouane and Melrhir (Vallès  
140 et al., 1997; Hamdi-Aïssa et al., 2004).

#### 141 3.2. *Spatial distribution of the mineralization*

142 The salinity of the phreatic aquifer varies considerably depending on the location (namely,  
143 the distance from wells or drains) and time (due to the influence of irrigation) (Fig. 5a).

144 Its salinity is low around irrigated and fairly well-drained areas, such as the palm groves of  
145 Hassi Miloud, just north of Ouargla (Fig. 3) that benefit from freshwater and are drained to the



146 sebkha Oum el Raneb. However, the three lowest salinity values are observed in the wells of  
147 Ouargla palm-grove itself, where the Phr aquifer watertable is deeper than 2 m.

148 Conversely, the highest salinity waters are found in wells drilled in the chotts and sebkhas (a  
149 sebkha is the central part of a chott where salinity is the largest) (Safioune and Oum er Raneb)  
150 where the aquifer is often shallower than 50 cm.

151 The salinity of the CT (Mio-pliocene) aquifer (Fig. 5b) is much lower than that of the Phr  
152 aquifer, and ranges from 1 to 2 g/L; however, its hardness is larger and it contains more sulfate,  
153 chloride and sodium than the waters of the Senonian formations and those of the CI aquifer. The  
154 salinity of the Senonian aquifer ranges from 1.1 to 1.7 g/L, while the average salinity of the CI  
155 aquifer is 0.7 g/L (Fig. 5c).

156 A likely contamination of the Mio-pliocene aquifer by phreatic groundwaters through casing  
157 leakage in an area where water is heavily loaded with salt and therefore particularly aggressive  
158 cannot be excluded.

### 159 3.3. Saturation Indices

160 The calculated saturation indices (SI) reveal that waters from CI at 50 °C are close to equi-  
161 librium with respect to calcite, except for 3 samples that are slightly oversaturated. They are  
162 however all undersaturated with respect to gypsum (Fig. 6).

163 Moreover, they are oversaturated with respect to dolomite and undersaturated with respect to  
164 anhydrite and halite (Fig. 7).

165 Waters from CT and phreatic aquifers show the same pattern, but some of them are more  
166 largely oversaturated with respect to calcite, at 25 °C.

167 However, several phreatic waters (P031, P566, PLX4, PL18, P002, P023, P116, P066, P162  
168 and P036) that are located in the sebkhas of Sefioune, Oum-er-Raneb, Bamendil and Ain el  
169 Beida's chott are saturated with gypsum and anhydrite. This is in accordance with highly evapo-  
170 rative environments found elsewhere (UNESCO, 1972; Hamdi-Aïssa et al., 2004; Slimani, 2006).

171 No significant trend of SI from south to north upstream and downstream of Oued Mya (Fig. 7)  
172 is observed. This suggests that the acquisition of mineralization is due to geochemical processes  
173 that have already reached equilibrium or steady state in the upstream areas of Ouargla.

### 174 3.4. Change of facies from the carbonated cluster to the evaporites' cluster

175 The facies shifts progressively from the carbonated (CI and CT aquifers) to the evaporites'  
176 one (Phr aquifer) with an increase in sulfates and chlorides at the expense of carbonates (SI of  
177 gypsum, anhydrite and halite). This is illustrated by a decrease of:  $[\text{HCO}_3^-]/([\text{Cl}^-] + 2[\text{SO}_4^{2-}])$   
178 (Fig. 8) from 0.2 to 0 and of  $[\text{SO}_4^{2-}]/[\text{Cl}^-]$  from 0.8 to values ranging from 0.3 and 0 (Fig. 9)  
179 while salinity increases. Carbonate concentrations tend towards very small values, while it is not  
180 the case for sulfates. This is due to both gypsum dissolution and calcite precipitation.

181 Chlorides in groundwater may come from three different sources: (i) ancient sea water en-  
182 trapped in sediments; (ii) dissolution of halite and related minerals that are present in evaporite  
183 deposits and (iii) dissolution of dry fallout from the atmosphere, particularly in these arid regions  
184 (Matiatos et al., 2014; Hadj-Ammar et al., 2014).

185  $[\text{Na}^+]/[\text{Cl}^-]$  ratio is from 0.85 to 1.26 for CI aquifer, from 0.40 to 1.02 for the CT aquifer  
186 and from 0.13 to 2.15 for the Phr aquifer. All the measured points from the three considered  
187 aquifers are more or less linearly scattered around the unity slope straight line that stands for  
188 halite dissolution (Fig. 10). The latter appears as the most dominant reaction occurring in the

189 medium. However, at very high salinity,  $\text{Na}^+$  seems to swerve from the straight line, towards  
190 smaller values.

191 A further scrutiny of Fig. 10 shows that CI waters are very close to the 1:1 line. CT waters  
192 are enriched in both  $\text{Na}^+$  and  $\text{Cl}^-$  but slightly lower than the 1:1 line while phreatic waters are  
193 largely enriched and much more scattered. CT waters are closer to the seawater mole ratio  
194 (0.858), but some lower values imply a contribution from another source of chloride than halite  
195 or from entrapped seawater. Conversely, a  $[\text{Na}^+]/[\text{Cl}^-]$  ratio larger than 1 is observed for phreatic  
196 waters, which implies the contribution of another source of sodium, most likely sodium sulfate,  
197 that is present as mirabilite or thenardite in the chotts and the sebkhas areas.

198  $[\text{Br}^-]/[\text{Cl}^-]$  ratio ranges from  $2 \times 10^{-3}$  to  $3 \times 10^{-3}$ . The value of this molar ratio for halite is  
199 around  $2.5 \times 10^{-3}$ , which matches the aforementioned range and confirms that halite dissolution  
200 is the most dominant reaction taking place in the studied medium.

201 In the CI, CT and Phr aquifers, calcium originates both from carbonate and sulfate (Fig. 11  
202 and 12). Three samples from CI aquifer are close to the  $[\text{Ca}^{2+}]/[\text{HCO}_3^-]$  1:2 line, while calcium  
203 sulfate dissolution explains the excess of calcium. However, nine samples from phreatic aquifer  
204 are depleted in calcium, and plot under the  $[\text{Ca}^{2+}]/[\text{HCO}_3^-]$  1:2 line. This cannot be explained  
205 by precipitation of calcite, as some are undersaturated with respect to that mineral, while others  
206 are oversaturated.

207 In this case, a cation exchange process seems to occur and lead to a preferential adsorption  
208 of divalent cations, with a release of  $\text{Na}^+$ . This is confirmed by the inverse modeling that is  
209 developed below and which implies  $\text{Mg}^{2+}$  fixation and  $\text{Na}^+$  and  $\text{K}^+$  releases.

210 Larger sulfate values observed in the phreatic aquifer (Fig. 12) with  $[\text{Ca}^{2+}]/[\text{SO}_4^{2-}] < 1$  can  
211 be attributed to a Na-Mg sulfate dissolution from a mineral bearing such elements. This is for  
212 instance the case of bloedite.

213

### 214 3.5. Isotope geochemistry

215 CT and CI aquifer exhibit depleted and homogeneous  $^{18}\text{O}$  contents, ranging from  $-8.32\text{‰}$   
216 to  $-7.85\text{‰}$ . This was already previously reported by many authors (Edmunds et al., 2003;  
217 Guendouz et al., 2003; Moulla et al., 2012). On the other hand,  $^{18}\text{O}$  values for the phreatic  
218 aquifer are widely dispersed and vary between  $-8.84\text{‰}$  to  $3.42\text{‰}$  (Table 6). Waters located  
219 north of the virtual line connecting approximately Hassi-Miloud to sebkhet Safioune, are found  
220 more enriched in heavy isotopes and are thus more evaporated. In that area, water table is close to  
221 the surface and mixing of both CI and CT groundwaters with phreatic ones through irrigation is  
222 nonexistent. Conversely, waters located south of Hassi Miloud up to Ouargla city show depleted  
223 values. This is the clear fingerprint of a contribution to the Phr waters from the underlying CI  
224 and CT aquifers (Gonfiantini et al., 1975; Guendouz, 1985; Fontes et al., 1986; Guendouz and  
225 Moulla, 1996).

226 Phreatic waters result from a mixing of two end-members. An evidence for this is given by  
227 considering the  $([\text{Cl}^-], ^{18}\text{O})$  relationship (Fig. 13). The two clusters are: i) a first cluster of  $^{18}\text{O}$   
228 depleted groundwater (Fig. 14), and ii) another cluster of  $^{18}\text{O}$  enriched groundwater with positive  
229 values and a high salinity. The latter is composed of phreatic waters occurring in the northern  
230 part of the study region.

231 Cluster I represents the waters from CI and CT whose isotopic composition is depleted  
232 in  $^{18}\text{O}$  (average value around  $-8.2\text{‰}$ ) (Fig. 13). They correspond to an old water recharge  
233 (palæorecharge); whose age estimated by means of  $^{14}\text{C}$ , exceeds 15.000 years BP (Guendouz,

234 1985; Guendouz and Michelot, 2006). So, it is not a water body that is recharged by recent  
 235 precipitation. It consists of CI and CT groundwaters and partly of phreatic waters, and can be  
 236 ascribed to an upward leakage favored by the extension of faults near Amguid El-Biod dorsal.

237 Cluster II, observed in Sebkhet Safioune, can be ascribed to the direct dissolution of surficial  
 238 evaporitic deposits conveyed by evaporated rainwater.

239 Evaporation alone cannot explain the distribution of data that is observed (Fig. 13). An  
 240 evidence for this is given in a semi-logarithmic plot (Fig. 14), as classically obtained according  
 241 to the simple approximation of Rayleigh equation (cf. Appendix):

$$\delta^{18}O \approx 1000 \times (1 - \alpha) \log[Cl^-] + cte, \quad (1)$$

$$\approx -\epsilon \log[Cl^-] + cte, \quad (2)$$

242 where  $\alpha$  is the fractionation factor during evaporation,  $\epsilon \equiv -1000 \times (1 - \alpha)$  is the enrichment  
 243 factor and K is a constant (Ma et al., 2010; Chkir et al., 2009).

244 CI and CT waters are better separated in the semi-logarithmic plot because they are differen-  
 245 tiated by their chloride content. According to equation (1), simple evaporation gives a straight  
 246 line (solid line in Fig. 14). The value of  $\epsilon$  used is the value at 25 °C, which is equal to -73.5.

247 P115 is the only sample that appears on the straight evaporation line (Fig. 14). It should be  
 248 considered as an outlier since the rest of the samples are all well aligned on the logarithmic fit  
 249 derived from the mixing line of Figure 13.

250 The phreatic waters that are close to cluster I (Fig. 13) correspond to groundwaters oc-  
 251 ccurring in the edges of the basin (Hassi Miloud, piezometer P433) (Fig. 14). They are low-  
 252 mineralized and acquire their salinity via two processes, namely: dissolution of evaporites along  
 253 their underground transit up to Sebkhet Safioune and dilution through upward leakage by the  
 254 less-mineralized waters of CI and CT aquifers (for example Hedeb I for CI and D7F4 for CT)  
 255 (Fig. 14) (Guendouz, 1985; Guendouz and Moulla, 1996).

256 The rates of the mixing that are due to upward leakage from CI to CT towards the phreatic  
 257 aquifer can be calculated by means of a mass balance equation. It only requires knowing the  $\delta$   
 258 values of each fraction that is involved in the mixing process.

259 The  $\delta$  value of the mixture is given by:

$$\delta_{\text{mix}} = f \times \delta_1 + (1 - f) \times \delta_2 \quad (3)$$

260 where  $f$  is the fraction of CI aquifer,  $1 - f$  the fraction of the CT and  $\delta_1, \delta_2$  are the respective  
 261 isotope contents.

262 Average values of mixing fractions from each aquifer to the phreatic waters computed by  
 263 means of equation (3) gave the rates of 65 % for CI aquifer and 35% for CT aquifer.

264 A mixture of a phreatic water component that is close to cluster I (*i.e.* P433) with another  
 265 component which is rather close to cluster II (*i.e.* P039) (Fig. 13 and 14), for an intermediate  
 266 water with a  $\delta^{18}O$  signature ranging from -5 ‰ to -2 ‰ gives mixture fraction values of 52 %  
 267 for cluster I and 48 % for cluster II. Isotope results will be used to independently cross-check the  
 268 validity of the mixing fractions derived from an inverse modeling involving chemical data (*cf.*  
 269 *infra.* 3.6.).

270 Turonian evaporites are found to lie in between CI deep aquifer and the Senonian and Miocene  
 271 formations bearing CT aquifer. CT waters can thus simply originate from ascending CI waters  
 272 that dissolve Turonian evaporites, a process which does not involve any change in  $^{18}O$  content.  
 273 Conversely, phreatic waters result to a minor degree from evaporation and mostly from dissolu-  
 274 tion of sebkhas evaporites by  $^{18}O$  enriched rainwater and mixing with CI-CT waters.

275 *3.5.1. Tritium content of water*

276 Tritium contents of Phr aquifer are relatively small (Table 6), they vary between 0 and 8 TU.  
277 Piezometers PZ12, P036 and P068 show values close to 8 TU, piezometers P018, P019, P416,  
278 P034, P042 and P093 exhibit values ranging between 5 and 6 TU, and the rest of the samples'  
279 concentrations are lower than 2 TU.

280 These values are dated back to November 1992 so they are old values and they are considered  
281 high comparatively to what is expected to be found nowadays. In fact, at present times, tritium  
282 figures have fallen lower than 5 TU in precipitation measured in the northern part of the country.

283 Tritium content of precipitation was measured as 16 TU in 1992 on a single sample that was  
284 collected from the National Agency for Water Resources station in Ouargla. A major part of  
285 this rainfall evaporates back into the atmosphere that is unsaturated in moisture. Consequently,  
286 enrichment in tritium happens as water evaporates back. The lightest fractions (isotopes) are  
287 the ones that escape first causing enriching the remaining fraction in tritium. The 16 TU value  
288 would thus correspond to a rainy event that had happened during the field campaign (5, 6 Nov.  
289 1992). It is the most representative value for that region and for that time. Unfortunately, all the  
290 other stations (Algiers, Ankara, and Tenerife) (Martinelli et al., 2014) are subject to a completely  
291 different climatic regime and besides the fact that they have more recent values, can absolutely  
292 not be used for our case. Therefore all the assumptions based on recent tritium rain values do not  
293 apply to this study.

294 Depleted contents in  $^{18}\text{O}$  and low tritium concentrations for phreatic waters fit well the mix-  
295 ing scheme and confirm the contribution from the older and deeper CI/CT groundwaters. The  
296 affected areas were clearly identified in the field and correspond to locations that are subject to  
297 a recycling and a return of irrigation waters whose origin are CI/CT boreholes. Moreover, the  
298 mixing that is clearly brought to light by the  $\text{Cl}^-$  vs.  $^{18}\text{O}$  diagrams (Fig. 13 and 14) could partly  
299 derive from an ascending drainage from the deep and confined CI aquifer (exhibiting depleted ho-  
300 mogenous  $^{18}\text{O}$  contents and very low tritium), a vertical leakage that is favoured by the Amguid  
301 El-biod highly faulted area (Guendouz and Moulla, 1996; Edmunds et al., 2003; Guendouz et al.,  
302 2003; Moulla et al., 2012).

303 *3.6. Inverse modeling*

304 We assume that the relationship between  $^{18}\text{O}$  and  $\text{Cl}^-$  data obtained in 1992 is stable with  
305 time, which is a logical assumption as times of transfer from CI to both CT and Phr are very long.  
306 Considering both  $^{18}\text{O}$  and  $\text{Cl}^-$  data, CI, CT and Phr data populations can be categorized. The CI  
307 and CT do not show appreciable  $^{18}\text{O}$  variations, and can be considered as a single population. The  
308 Phr samples consist however of different populations: cluster I, with  $\delta^{18}\text{O}$  values close to -8, and  
309 small  $\text{Cl}^-$  concentrations, more specifically less than  $35 \text{ mmol L}^{-1}$ ; cluster II, with  $\delta^{18}\text{O}$  values  
310 larger than 3, and very large  $\text{Cl}^-$  concentrations, more specifically larger than  $4,000 \text{ mmol L}^{-1}$   
311 (Table 7); intermediate Phr samples result from mixing between clusters I and II (mixing line in  
312 Fig. 13, mixing curve in Fig. 14) and from evaporation of cluster I (evaporation line in Fig. 14).

313 The mass-balance modeling has shown that relatively few phases are required to derive ob-  
314 served changes in water chemistry and to account for the hydrochemical evolution in Ouargla's  
315 region. The mineral phases' selection is based upon geological descriptions and analysis of rocks  
316 and sediments from the area (OSS, 2003; Hamdi-Aïssa et al., 2004).

317 The inverse model was constrained so that mineral phases from evaporites including gypsum,  
318 halite, mirabilite, glauberite, sylvite and bloedite were set to dissolve until they reach saturation,  
319 and calcite, dolomite were set to precipitate once they reached saturation. Cation exchange reac-  
320 tions of  $\text{Ca}^{2+}$ ,  $\text{Mg}^{2+}$ ,  $\text{K}^+$  and  $\text{Na}^+$  on exchange sites were included in the model to check which

321 cations are adsorbed or desorbed during the process. Dissolution and desorption contribute as  
322 positive terms in the mass balance, as elements are released in solution. On the other hand,  
323 precipitation and adsorption contribute as negative terms, while elements removed from the so-  
324 lution.  $\text{CO}_{2(g)}$  dissolution is considered by Phreeqc as a dissolution of a mineral, whereas  $\text{CO}_{2(g)}$   
325 degassing is dealt with as if it were a mineral precipitation.

326 Inverse modelling leads to a quantitative assessment of the different solutes' acquisition pro-  
327 cesses and a mass balance for the salts that are dissolved or precipitated from CI, CT and Phr  
328 groundwaters (Fig. 14, Table 8), as follows:

- 329 • transition from CI to CT involves gypsum, halite and sylvite dissolution, and some ion  
330 exchange namely calcium and potassium fixation on exchange sites against magnesium  
331 release, with a very small and quite negligible amount of  $\text{CO}_{2(g)}$  degassing. The maximum  
332 elemental concentration fractional error equals 1%. The model consists of a minimum  
333 number of phases (*i.e.* 6 solid phases and  $\text{CO}_{2(g)}$ ); Another model implies as well dolomite  
334 precipitation with the same fractional error;
- 335 • transition from CT to an average water component of cluster I involves dissolution of  
336 halite, sylvite, and bloedite from Turonian evaporites, with a very tiny calcite precipitation.  
337 The maximum fractional error in elemental concentration is 4%. Another model implies  
338  $\text{CO}_{2(g)}$  escape from the solution, with the same fractional error. Large amounts of  $\text{Mg}^{2+}$   
339 and  $\text{SO}_4^{2-}$  are released within the solution (Sharif et al., 2008; Li et al., 2010; Carucci  
340 et al., 2012);
- 341 • the formation of Phr cluster II can be modeled as being a direct dissolution of salts from the  
342 sebkha by rainwater with positive  $\delta^{18}\text{O}$ ; the most concentrated water (P036 from Sebkhet  
343 Safioune) is taken here for cluster II, and pure water as rainwater. In a descending order  
344 of amount, halite, sylvite, gypsum and huntite are the minerals that are the most involved  
345 in the dissolution process. A small amount of calcite precipitates while some  $\text{Mg}^{2+}$  are  
346 released versus  $\text{K}^+$  fixation on exchange sites. The maximum elemental fractional error in  
347 the concentration is equal to 0.004%. Another model implies dolomite precipitation with  
348 some more huntite dissolving, instead of calcite precipitation, but salt dissolution and ion  
349 exchange are the same. Huntite, dolomite and calcite stoichiometries are linearly related,  
350 so both models can fit field data, but calcite precipitation is preferred compared to dolomite  
351 precipitation at low temperature;
- 352 • the origin of all phreatic waters can be explained by a mixing in variable proportions  
353 of cluster I and cluster II. For instance, waters from cluster I and cluster II can easily be  
354 separated by their  $\delta^{18}\text{O}$  respectively close to  $-8\text{‰}$  and  $3.5\text{‰}$  (Fig. 13 and 14). Mixing the  
355 two clusters is of course not an inert reaction, but rather results in the dissolution and the  
356 precipitation of minerals. Inverse modeling is then used to compute both mixing rates and  
357 the extent of matter exchange between soil and solution. For example, a phreatic water  
358 (piezometer P068) with intermediate values ( $\delta^{18}\text{O} = -3$  and  $[\text{Cl}^-] \approx 2\text{ M}$ ) is explained  
359 by the mixing of 58% water from cluster I and 42% from cluster II. In addition, calcite  
360 precipitates,  $\text{Mg}^{2+}$  fixes on exchange sites, against  $\text{Na}^+$  and  $\text{K}^+$ , gypsum dissolves as well  
361 as a minor amount of huntite (Table 8). The maximum elemental concentration fractional  
362 error is 2.5% and the mixing fractions' weighted the  $\delta^{18}\text{O}$  is  $-3.17\text{‰}$ , which is very  
363 close to the measured value ( $-3.04\text{‰}$ ). All the other models, making use of a minimum  
364 number of phases, and not taking into consideration ion exchange reactions are not found

365 compatible with isotope data. Mixing rates obtained with such models are for example  
366 98% of cluster I and 0.9% of cluster II, which leads to a  $\delta^{18}O = (-7.80 \text{‰})$  which is quite  
367 far for the real measured value ( $-3.04 \text{‰}$ ).

368 The main types of groundwaters occurring in Ouargla basin are thus explained and could  
369 quantitatively be reconstructed. An exception is however sample P115, which is located exactly  
370 on the evaporation line of Phr cluster I. Despite numerous attempts, it could not be quantitatively  
371 rebuilt. Its  $^3H$  value (6.8) indicates that it is derived from a more or less recent water component  
372 with very small salt content, most possibly affected by rainwater and some preferential flow  
373 within the piezometer. As this is the only sample on this evaporation line, there remains a doubt  
374 on its significance.

375 Globally, the summary of mass transfer reactions occurring in the studied system (Table 8)  
376 shows that gypsum dissolution results in calcite precipitation and  $CO_{2(g)}$  dissolution, thus acting  
377 as an inorganic carbon sink.

#### 378 4. CONCLUSIONS

379 Groundwater hydrochemistry is a good record indicator for the water-rock interactions that  
380 occur along the groundwater flowpath. The mineral load reflects well the complex processes  
381 taking place while water circulates underground since its point of infiltration.

382 The hydrochemical study of the aquifer system occurring in Ouargla's basin allowed us to  
383 identify the origin of its mineralization. Waters exhibit two different facies: sodium chloride and  
384 sodium sulfate for the phreatic aquifer (Phr), sodium sulfate for the Complexe Terminal (CT)  
385 aquifer and sodium chloride for the Continental Intercalaire (CI) aquifer. Calcium carbonate  
386 precipitation and evaporite dissolution explain the facies change from carbonate to sodium chlo-  
387 ride or sodium sulfate. However reactions imply many minerals with common ions, deep reac-  
388 tions without evaporation as well as shallow processes affected by both evaporation and mixing.  
389 Those processes are separated by considering both chemical and isotopic data, and quantitatively  
390 explained making use of an inverse geochemical modeling. The main result is that Phr waters  
391 do not originate simply from infiltration of rainwater and dissolution of salts from the sebkhas.  
392 Conversely, Phr waters are largely influenced by the upwardly mobile deep CT and CI groundwa-  
393 ters, fractions of the latter interacting with evaporites from Turonian formations. Phreatic waters  
394 occurrence is explained as a mixing of two end-member components: cluster I, which is very  
395 close to CI and CT, and cluster II, which is highly mineralized and results from the dissolution  
396 by rainwater of salts from the sebkhas.

397 At depth, CI leaks upwardly and dissolves gypsum, halite and sylvite, with some ion ex-  
398 change, to give waters of CT aquifer composition.

399 CT transformation into Phr cluster I waters involves the dissolution of Turonian evaporites  
400 (halite, sylvite and bloedite) with minor calcite precipitation.

401 At the surface, direct dissolution by rainwater of salts from sebkhas (halite, sylvite, gypsum  
402 and some huntite) with precipitation of calcite and  $Mg^{2+}/K^+$  ion exchange results in cluster II  
403 Phr composition.

404 All phreatic groundwaters result from a mixing of cluster I and cluster II water that is accom-  
405 panied by calcite precipitation, fixation of  $Mg^{2+}$  on ion exchange sites against the release of  $K^+$   
406 and  $Na^+$ .

407 Moreover, some  $CO_{2(g)}$  escapes from the solution at depth, but dissolves much more at the  
408 surface. The most complex phenomena occur during the dissolution of Turonian evaporites while

409 CI leaks upwardly towards CT, and from Phr I to Phr II, while the transition from CT to Phr I  
 410 implies a very limited number of phases. Globally, gypsum dissolution and calcite precipitation  
 411 processes both act as an inorganic carbon sink.

#### 412 ACKNOWLEDGEMENTS

413 The authors wish to thank the staff members of the National Agency for Water Resources  
 414 in Ouargla (ANRH) and the Laboratory of Algerian Waters (ADE) for the support provided to  
 415 the Technical Cooperation programme within which this work was carried out. Analyses of  
 416  $^{18}\text{O}$  were funded by the project CDTN / DDHI (Guendouz and Moulla, 1996). The supports of  
 417 University of Ouargla and of INRA for travel grants of R. Slimani and G. Bourrié are gratefully  
 418 acknowledged too.

#### 419 APPENDIX

420 According to a simple Rayleigh equation, the evolution of the heavy isotope ratio in the  
 421 remaining liquid  $R_l$  is given by:

$$R_l \approx R_{l,0} \times f_l^{\alpha-1}, \quad (4)$$

422 where  $f_l$  is the fraction remaining liquid and  $\alpha$  the fractionation factor.

423 The fraction remaining liquid is derived from chloride concentration, as chloride can be con-  
 424 sidered as conservative during evaporation: all phreatic waters are undersaturated with respect to  
 425 halite, that precipitates only in the last stage. Hence, the following equation holds:

$$f_l \equiv \frac{n_{w,1}}{n_{w,0}} = \frac{[\text{Cl}^-]_0}{[\text{Cl}^-]_1}. \quad (5)$$

426 By taking natural logarithms, one obtains:

$$\ln R_l \approx (1 - \alpha) \times \ln[\text{Cl}^-] + cte, \quad (6)$$

427 As, by definition,

$$R_l \equiv R_{std.} \times \left(1 + \frac{\delta^{18}\text{O}}{1000}\right), \quad (7)$$

428 one has:

$$\ln R_l \equiv \ln R_{std.} + \ln\left(1 + \frac{\delta^{18}\text{O}}{1000}\right), \quad (8)$$

$$\approx \ln R_{std.} + \frac{\delta^{18}\text{O}}{1000}, \quad (9)$$

429 hence, with base 10 logarithms:

$$\delta^{18}\text{O} \approx 1000(1 - \alpha) \log[\text{Cl}^-] + cte, \quad (10)$$

$$\approx -\epsilon \log[\text{Cl}^-] + cte, \quad (11)$$

430 where as classically defined  $\epsilon = 100(\alpha - 1)$  is the enrichment factor.

431 **References**

- 432 Al-Gamal, S.A., 2011. An assessment of recharge possibility to North-Western Sahara Aquifer System (NWSAS) using  
 433 environmental isotopes. *Journal of Hydrology* 398, 184 – 190.
- 434 ANRH, 2011. Inventaire des forages de la Wilaya de Ouargla. Rapport technique. Agence Nationale des Ressources  
 435 Hydrauliques.
- 436 Aumassip, G., Dagorne, A., Estorges, P., Lefèvre-Witier, P., Mahrour, F., Nesson, C., Rouvillois-Brigol, M., Trecolle, G.,  
 437 1972. Aperçus sur l'évolution du paysage quaternaire et le peuplement de la région de Ouargla. *Libyca*, 205–257.
- 438 Belkhir, L., Boudoukha, A., Mouni, L., Baouz, T., 2010. Application of multivariate statistical methods and inverse  
 439 geochemical modeling for characterization of groundwater — A case study: Ain Azel plain (Algeria). *Geoderma*  
 440 159, 390 – 398.
- 441 Belkhir, L., Mouni, L., Boudoukha, A., 2012. Geochemical evolution of groundwater in an alluvial aquifer: Case of El  
 442 Eulma aquifer, East Algeria. *Journal of African Earth Sciences* 66–67, 46 – 55.
- 443 Carucci, V., Petitta, M., Aravena, R., 2012. Interaction between shallow and deep aquifers in the Tivoli Plain (Central  
 444 Italy) enhanced by groundwater extraction: A multi-isotope approach and geochemical modeling. *Applied Geochem-*  
 445 *istry* 27, 266 – 280. URL: <http://www.sciencedirect.com/science/article/pii/S0883292711004628>,  
 446 doi:<http://dx.doi.org/10.1016/j.apgeochem.2011.11.007>.
- 447 Chellat, S., Bourefis, A., Hamdi-Aïss, a.B., Djerrab, A., 2014. Paléoenvironnemental reconstitution of Mio-pliocenes  
 448 sandstones of the lower-Sahara at the base of exoscopic and sequential analysis. *Pensee Journal* 76, 34 – 51.
- 449 Chkir, N., Guendouz, A., Zouari, K., Hadj Ammar, F., Moulla, A., 2009. Uranium isotopes in groundwater from the  
 450 continental intercalaire aquifer in Algerian Tunisian Sahara (Northern Africa). *Journal of Environmental Radioac-*  
 451 *tivity* 100, 649 – 656. URL: <http://www.sciencedirect.com/science/article/pii/S0265931X09001143>,  
 452 doi:<http://dx.doi.org/10.1016/j.jenvrad.2009.05.009>.
- 453 Cornet, A., Gouscov, N., 1952. Les eaux du Crétacé inférieur continental dans le Sahara algérien: nappe dite "Albien",  
 454 in: *Congrès géologique international, Alger*. p. 30.
- 455 Dai, Z., Samper, J., Ritzi, R., 2006. Identifying geochemical processes by inverse modeling of multicomponent reactive  
 456 transport in the aquia aquifer. *Geosphere* 2, 210–219.
- 457 Deutsch, W., 1997. *Groundwater Chemistry-Fundamentals and Applications to Contamination*. New York.
- 458 Dubief, J., 1953. *Essai sur l'hydrologie superficielle au Sahara*. Direction du service de la colonisation et de  
 459 l'hydraulique, Service des études scientifiques.
- 460 Dubief, J., 1963. *Le climat du Sahara*. Hors-série, Institut de recherches sahariennes.
- 461 Eckstein, G., Eckstein, Y., 2003. A hydrogeological approach to transboundary ground water resources and international  
 462 law. *American University International Law Review* 19, 201–258.
- 463 Edmunds, W., Guendouz, A., Mamou, A., Moulla, A., Shand, P., Zouari, K., 2003. Groundwater evolution in the  
 464 continental intercalaire aquifer of southern Algeria and Tunisia: trace element and isotopic indicators. *Applied*  
 465 *Geochemistry* 18, 805–822.
- 466 Fontes, J., Yousfi, M., Allison, G., 1986. Estimation of long-term, diffuse groundwater discharge in the northern sahara  
 467 using stable isotope profiles in soil water. *Journal of Hydrology* 86, 315 – 327.
- 468 Foster, S., Margat, J., Droubi, A., 2006. Concept and importance of nonrenewable resources. Number 10 in IHP-VI  
 469 Series on Groundwater, UNESCO.
- 470 Furon, R., 1960. *Géologie de l'Afrique*. 2eme édition, Payot.
- 471 Güler, C., Thyne, G., 2004. Hydrologic and geologic factors controlling surface and groundwater chemistry in Indian  
 472 wells–Owens valley area, southeastern California, USA. *Journal of Hydrology* 285, 177–198.
- 473 Gonfiantini, R., Conrad, G., Fontes, J.C., Sauzay, G., Payne, B., 1975. Étude isotopique de la nappe du Continental  
 474 Intercalaire et de ses relations avec les autres nappes du Sahara septentrional. *Isotope Techniques in Groundwater*  
 475 *Hydrology* 1, 227–241.
- 476 Guendouz, A., 1985. Contribution à l'étude hydrochimique et isotopique des nappes profondes du Sahara nord-est  
 477 septentrional, Algérie. Phd thesis. Université d'Orsay, France.
- 478 Guendouz, A., Michelot, J., 2006. Chlorine-36 dating of deep groundwater from northern Sahara. *Journal of Hydrology*  
 479 328, 572–580.
- 480 Guendouz, A., Moulla, A., 1996. Étude hydrochimique et isotopique des eaux souterraines de la cuvette de Ouargla,  
 481 Algérie. Rapport technique. CDTN/DDHI.
- 482 Guendouz, A., Moulla, A., Edmunds, W., Zouari, K., Shands, P., Mamou, A., 2003. Hydrogeochemical and isotopic  
 483 evolution of water in the complex terminal aquifer in Algerian Sahara. *Hydrogeology Journal* 11, 483–495.
- 484 Hadj-Ammar, F., Chkir, N., Zouari, K., Hamelin, B., Deschamps, P., Aigoun, A., 2014. Hydro-  
 485 geochemical processes in the Complexe Terminal aquifer of southern Tunisia: An integrated investi-  
 486 gation based on geochemical and multivariate statistical methods. *Journal of African Earth Sciences*  
 487 100, 81 – 95. URL: <http://www.sciencedirect.com/science/article/pii/S1464343X14001940>,  
 488 doi:<http://dx.doi.org/10.1016/j.jafrearsci.2014.06.015>.



489 Hamdi-Aïssa, B., Vallès, V., Aventurier, A., Ribolzi, O., 2004. Soils and brines geochemistry and mineralogy of hyper  
490 arid desert playa, Ouargla basin, Algerian Sahara. *Arid Land Research and Management* 18, 103–126.

491 Kenoyer, G., Bowser, C., 1992. Groundwater chemical evolution in a sandy aquifer in northern Wisconsin. *Water*  
492 *Resources Research* 28, 591–600.

493 Kuells, C., Adar, E., Udluft, P., 2000. Resolving patterns of ground water flow by inverse hydrochemical modeling in a  
494 semiarid Kalahari basin. *Tracers and Modelling in Hydrogeology* 262, 447–451.

495 Le Houérou, H., 2009. *Bioclimatology and biogeography of Africa*. Springer Verlag.

496 Lelièvre, R., 1969. Assainissement de la cuvette de Ouargla. rapports Géohydraulique n° 2. Ministère des Travaux  
497 Publics et de la construction.

498 Li, P., Qian, H., Wu, J., Ding, J., 2010. Geochemical modeling of groundwater in southern plain area of Pengyang  
499 County, Ningxia, China. *Water Science and Engineering* 3, 282–291.

500 Ma, J., Pan, F., Chen, L., Edmunds, W., Ding, Z., Zhou, K., He, J., Zhou, K., Huang, T., 2010. Isotopic and geochemical  
501 evidence of recharge sources and water quality in the Quaternary aquifer beneath Jinchang city, NW China. *Applied*  
502 *Geochemistry* 25, 996–1007.

503 Martinelli, G., Chahoud, A., Dadomo, A., Fava, A., 2014. Isotopic features of emilia-romagna region  
504 (north italy) groundwaters: Environmental and climatological implications. *Journal of Hydrology* 519, Part  
505 B, 1928 – 1938. URL: <http://www.sciencedirect.com/science/article/pii/S0022169414007690>,  
506 doi:<http://dx.doi.org/10.1016/j.jhydrol.2014.09.077>.

507 Matiatos, I., Alexopoulos, A., Godelitsas, A., 2014. Multivariate statistical analysis of the hydrogeochemical and isotopic  
508 composition of the groundwater resources in northeastern Peloponnesus (Greece). *Science of The Total Environment*  
509 476–477, 577 – 590. URL: <http://www.sciencedirect.com/science/article/pii/S0048969714000515>,  
510 doi:<http://dx.doi.org/10.1016/j.scitotenv.2014.01.042>.

511 Moulias, D., 1927. L'eau dans les oasis sahariennes, organisation hydraulique, régime juridique. Phd thesis. Alger.

512 Moulla, A., Guendouz, A., Cherchali, M.H., Chaid, Z., Ouarezki, S., 2012. Updated geochemical and isotopic data  
513 from the Continental Intercalaire aquifer in the Great Occidental Erg sub-basin (south-western Algeria). *Quaternary*  
514 *International* 257, 64–73.

515 OECD, 2008. *OECD Environmental Outlook to 2030. Technical Report 1*. Organisation for Economic Cooperation and  
516 Development.

517 ONM, 1975/2013. *Bulletins mensuels de relevé des paramètres climatologiques en Algérie*. Office national  
518 météorologique.

519 OSS, 2003. *Système aquifère du Sahara septentrional*. Technical Report. Observatoire du Sahara et du Sahel.

520 OSS, 2008. *Système aquifère du Sahara septentrional (Algérie, Tunisie, Libye): gestion concertée d'un bassin trans-*  
521 *frontalier*. Technical Report 1. Observatoire du Sahara et du Sahel.

522 Ould Baba Sy, M., Besbes, M., 2006. Holocene recharge and present recharge of the Saharan aquifers — a study by  
523 numerical modeling, in: *International symposium - Management of major aquifers*.

524 Parkhurst, D., Appelo, C., 2013. *Description of Input and Examples for PHREEQC (Version 3) — A computer program*  
525 *for speciation, batch-reaction, one-dimensional transport, and inverse geochemical calculations*. Technical Report 6.  
526 U.S. Department of the Interior, U.S. Geological Survey. URL: <http://pubs.usgs.gov/tm/06/a43>.

527 Plummer, L., Back, M., 1980. The mass balance approach: application to interpreting the chemical evolution of hydro-  
528 logical systems. *American Journal of Science* 280, 130–142.

529 Plummer, L., Sprinkle, C., 2001. Radiocarbon dating of dissolved inorganic carbon in groundwater from confined parts  
530 of the upper Floridan aquifer, Florida, USA. *Journal of Hydrology* 9, 127–150.

531 Sharif, M., Davis, R., Steele, K., Kim, B., Kresse, T., Fazio, J., 2008. Inverse geochemical modeling of groundwater  
532 evolution with emphasis on arsenic in the Mississippi River Valley alluvial aquifer, Arkansas (USA). *Journal of Hy-*  
533 *drology* 350, 41 – 55. URL: <http://www.sciencedirect.com/science/article/pii/S0022169407007093>,  
534 doi:<http://dx.doi.org/10.1016/j.jhydrol.2007.11.027>.

535 Slimani, R., 2006. Contribution à l'évaluation d'indicateurs de pollution environnementaux dans la région de Ouargla:  
536 cas des eaux de rejets agricoles et urbaines. Master's thesis. Université de Ouargla.

537 Stumm, W., Morgan, J., 1999. *Aquatic Chemistry: Chemical Equilibria and Rates in Natural Waters*. John Wiley and  
538 Sons.

539 Thomas, J., Welch, A., Preissler, A., 1989. Geochemical evolution of ground water in smith creek valley - a hydrologi-  
540 cally closed basin in central Nevada, USA. *Applied Geochemistry* 4, 493–510.

541 UNESCO, 1972. *Projet ERESS, Étude des ressources en eau du Sahara septentrional*. Technical Report 10. UNESCO.

542 Vallès, V., Rezagui, M., Auque, L., Semadi, A., Roger, L., Zouggari, H., 1997. Geochemistry of saline soils in two arid  
543 zones of the Mediterranean basin. I. Geochemistry of the Chott Melghir-Mehrouane watershed in Algeria. *Arid Soil*  
544 *Research and Rehabilitation* 11, 71–84.

Table 1: Field and analytical data for the Continental Intercalaire aquifer.

Locality	Lat.	Long.	Elev.	Date	EC	T	pH	/mmolL <sup>-1</sup>									
								Alk	Cl <sup>-</sup>	SO <sub>4</sub> <sup>2-</sup>	Na <sup>+</sup>	K <sup>+</sup>	Mg <sup>2+</sup>	Ca <sup>2+</sup>	Br <sup>-</sup>		
Hedbb I	3,534,750	723,986	134.8	09/11/2012	2.01	46.5	7.65	3.5	5.8	6.79	10.7	0.63	2.49	3.3			
Hedbb I	3,534,750	723,986	134.8	1992	1.9	49.3	7.35	0.42	5.81	1.07	5.71	0.18	0.77	0.48	0.034		
Hedbb II	3,534,310	724,290	146.2	1992	2.02	47.4	7.64	0.58	6.19	1.22	5.06	0.2	1.28	0.82			
Aoumet Mousa	3,548,896	721,076	132.6	1992	2.2	48.9	7.55	1.28	6.49	1.28	5.65	0.16	1.14	1.17			
Aoumet Mousa	3,548,896	721,076	132.6	22/02/2013	2.2	48.9	7.55	3.19	9.8	3.89	6.3	0.69	5.71	1.27			
Hedbb I	3,534,750	723,986	134.8	11/12/2010	2.19	49.3	7.35	1.91	12.4	4.58	10.7	0.7	3.77	2.35			
Hedbb II	3,534,310	724,290	146.2	1/12/2010	2.26	47.4	7.64	2.11	13.1	5.24	13.9	0.53	4.53	1.41			
Hedbb I	3,591,659	721,636	110	24/02/2013	2.43	50.5	6.83	2.98	14.3	5.24	10.8	0.84	3.44	4.63		0.033	
Hassi Khf	3,534,750	723,986	134.8	27/02/2013	2.01	46.5	7.65	3.46	15.1	7.67	11.8	0.51	5.57	5.16			
Hassi Khf	3,591,659	721,636	110	09/11/2012	2	50.1	7.56	3.31	15.3	7.77	12.2	0.59	5.77	4.95			
Hassi Khf	3,560,264	720,366	160	22/02/2013	2.96	54.5	7.34	2.58	18.6	6.21	20.6	0.66	4.79	1.38			

Table 2: Field and analytical data for the Complex Terminal aquifer.

Locality	Site	Aquifer	Lat.	Long.	Elev.	Date	EC	T	pH	Alk.	Cl <sup>-</sup>	SO <sub>4</sub> <sup>2-</sup>	Na <sup>+</sup>	K <sup>+</sup>	Mg <sup>2+</sup>	Ca <sup>2+</sup>	Br <sup>-</sup>
				/m			/mS cm <sup>-1</sup>	/°C					/mmol L <sup>-1</sup>				
Ramerdji	DIF4	M	3,560,759.6	720,586.2	206	20/01/2013	2.02	20.1	7.86	1.63	10.1	579	9.88	0.68	3.92	2.51	
Ramerdji	DIF5	M	3,567,891.7	720,586.2	206	19/02	2.02	21.1	8.2	1.96	10.75	3.54	10.88	0.99	2.32	2.12	
Ifr	DIF151	S	3,538,891.7	721,060.5	204	1992	2.67	23.5	7	1.26	10.75	2.71	7.99	0.73	2.32	2.12	
Saïd Ouba	D2F66	M	3,540,257.3	720,085.4	177	1992	2.31	18	8	1.43	11.02	4.73	11.47	0.16	2.07	3.33	
Oglat Larbaâ	D6F64	M	3,566,201.4	729,369.3	177	27/01/2013	2.31	24	7.9	1.41	11.36	6.85	11.59	2.31	1.96	4.58	
El-Bour	D4F94	M	3,536,245.2	722,641.7	100.6	1992	3.05	26.2	7.37	1.61	12.8	6.79	5.15	1.94	1.65	9.13	
Saïd Ouba I	D2F71	S	3,557,412.4	718,272.8	211.9	1992	2.27	24.2	8.2	1.54	13.53	5.72	14.99	0.33	3.28	2.57	
Deiche	D6F61	M	3,547,557.1	717,067.1	173.5	26/01/2013	2.22	22.9	7.74	1.78	14.2	8.41	12.6	0.66	3.38	4.43	
Saïd Ouba II	D2F71	M	3,557,412.4	718,272.8	211.9	1992	2.22	22.9	7.74	1.78	14.2	8.41	12.6	0.66	3.38	4.43	
Saïd Ouba I	D2F71	M	3,557,412.4	718,272.8	211.9	26/01/2013	5.63	25.1	7.34	2.38	14.3	6.86	13.1	0.4	3.36	5.43	0.034
Rouissat III	D3F10	S	3,535,068.1	722,552.1	248	20/01/2013	2.37	18.9	7.98	1.65	15.4	8.64	12.6	1.56	5.79	4.25	
Ifr	DIF151	S	3,538,891.7	721,060.5	204	27/01/2013	2.37	22.9	7.79	1.75	15.4	8.31	13.7	0.22	5.17	4.75	
Saïd Ouba	D2F66	M	3,540,257.3	720,085.4	216	31/01/2013	2.38	24.9	7.91	2.19	16.1	16.3	8.65	16.5	0.74	4.29	4.93
Oglat Larbaâ	D6F64	M	3,566,201.4	729,369.3	177	31/01/2013	2.43	23.7	7.62	2.3	16.3	8.65	16.1	0.68	0.71	5.86	
SAR Mekhadma	DIF91	S	3,536,257.7	717,822.3	221	03/02/2013	2.47	25.8	7.75	3.43	16.3	8.53	16.1	0.88	5.27	4.92	
Saïd Ouba	D6F61	M	3,547,557.1	717,067.1	173.5	25/01/2013	2.65	19.9	8.02	2.14	16.8	16.8	16.8	1.01	0.35	7.01	
Saïd Ouba	D6F61	M	3,547,557.1	717,067.1	173.5	25/01/2013	3.36	24.7	8.05	1.98	16.8	16.8	16.8	1.01	0.35	7.01	
A Louisa	D4F73	S	3,537,523.4	721,904.6	310	26/01/2013	2.57	24	7.49	1.98	17.4	9.04	13.9	1.99	5.78	5.05	0.033
Charzalet A.H	D6F79	M	3,598,750.2	720,356.8	119	02/02/2013	2.84	22.5	7.55	3.47	17.4	9.35	16.6	0.62	6.24	4.96	
Am moussa II	D9F30	S	3,537,814.1	719,665.1	220.6	02/02/2013	7.52	23.9	7.52	2.37	17.5	8.24	17.3	0.39	3.1	6.46	0.033
Am N'sara	D6F50	S	3,559,232.6	716,868.4	173	02/02/2013	2.62	23.8	7.65	2.11	17.7	9.19	15.5	1.13	6.11	4.73	
H.Miloud	DIF135	M	3,547,557.1	717,067.1	173.5	03/02/2013	2.76	21.6	7.55	3.32	17.9	9.22	16.5	1.01	6.17	4.91	
El Bour	D6F61	M	3,540,257.3	715,816.0	169	25/01/2013	2.65	19.9	8.02	2.14	17.9	5.28	15.8	1.6	3.84	4.73	
H.Miloud	DIF135	M	3,547,557.1	717,067.1	173.5	03/02/2013	2.65	19.9	8.02	2.14	17.9	5.28	15.8	1.6	3.84	4.73	
N'youssa El Hou	D6F51	S	3,556,256.7	718,976.5	198	31/01/2013	3.07	22.9	7.52	2.03	18.4	9.71	17.9	0.45	6.17	4.99	
El Koum	D6F67	S	3,573,694.1	721,639.7	143	1992	2.5	25	7.6	1.5	18.79	7.17	10.18	3.43	4.97	5.81	
El Koum	D6F67	S	3,573,694.1	721,639.7	143	1992	2.5	25	7.6	1.5	18.79	7.17	10.18	3.43	4.97	5.81	
ITAS	DIF150	M	3,536,186.6	717,046.1	93.1	21/01/2013	3.66	23.9	7.54	1.48	18.8	7.07	10.1	3.41	4.94	5.77	
Am moussa V	D9F13	M	3,538,409.2	718,680.2	210.2	08/02/2013	2.39	25.3	7.22	2.28	19.4	9.45	18.8	0.39	3.31	7.61	
El-Bour	D4F94	M	3,536,245.2	722,641.7	100.6	1992	2.3	21.2	7.9	1.58	20.05	7.21	12.09	2.62	5.76	5.17	
Rouissat I	D3F18	M	3,535,564.2	722,498.9	80.4	26/09/2013	2.13	21	7.84	1.85	21.26	11.46	17.2	0.78	5.08	6.01	
Rouissat I	D3F18	M	3,535,564.2	722,498.9	80.4	26/09/2013	2.13	21	7.84	1.85	21.26	11.46	17.2	0.78	5.08	6.01	
St. poupage ebott	D5F80	S	3,541,656.9	723,521.9	224.1	04/02/2013	3.28	24.5	8.23	3.91	22.1	11.9	19.9	2.13	7.64	6.28	
Chart Palmerate	D5F77	S	3,538,219.3	725,541.3	242.8	05/02/2013	3.37	24.6	7.53	3.26	22.3	12.1	20.9	2.15	8.25	5.78	
Bour El Hakeha	DIF134	M	3,545,233.1	720,391.7	86	05/02/2013	3.4	22.2	7.34	4.13	23.2	12.2	21.2	1.49	8.61	6.01	
Guet Chemia	D2F69	M	3,552,504.9	712,786.3	137.1	03/02/2013	3.54	24.6	7.61	2.24	24.7	12.7	21.1	1.65	8.45	6.47	
Abzatt	D2F69	M	3,552,504.9	712,786.3	137.1	03/02/2013	3.54	24.6	7.61	2.24	24.7	12.7	21.1	1.65	8.45	6.47	
Frame	D6F62	M	3,570,175.8	717,133.8	167.5	27/01/2013	3.79	24.2	7.95	2.27	25.9	13.5	22.6	0.64	8.91	7.16	
Am Issa	D6F62	M	3,570,175.8	717,133.8	167.5	27/01/2013	3.79	24.2	7.95	2.27	25.9	13.5	22.6	0.64	8.91	7.16	
N'youssa El Hou	D6F51	S	3,556,256.7	718,976.5	198	25/01/2013	3.15	23.2	8.05	2.59	28.59	8.61	23.14	0.62	4.42	8.01	0.035
N'youssa El Hou	D6F51	S	3,556,256.7	718,976.5	198	1992	3.15	23.2	8.05	2.59	28.59	8.61	23.14	0.62	4.42	8.01	
H.Miloud Benyaza	DIF138	M	3,551,192.5	717,042.1	88.9	28/01/2013	3.85	25.2	7.61	2.44	28.4	14.2	23.9	1.66	10.01	7.12	
Am L'aarab	D6F49	M	3,558,822.6	716,799.1	156.5	28/01/2013	3.97	23.7	7.33	2.16	28.4	14.2	23.9	1.66	10.01	7.12	
H.Miloud Benyaza	DIF138	M	3,551,192.5	717,042.1	88.9	1992	2.9	22.8	7.5	2.16	28.92	9.03	23.87	0.52	4.99	7.7	0.037
Rouissat	D3F8	M	3,545,470.7	732,837.6	332.4	03/02/2013	4.38	25.4	7.51	1.71	29.8	8.33	22.8	1.23	6.23	6.08	
Rouissat	D3F8	M	3,545,470.7	732,837.6	332.4	1992	6.16	25.3	7.22	1.71	29.81	8.33	22.86	1.23	6.23	6.08	
Am El Aech	D3F8	M	3,544,683.6	733,130	331.6	1992	6.16	25.3	7.22	1.71	29.81	8.33	22.86	1.23	6.23	6.08	
St. poupage ebott	D3F80	S	3,541,666.9	723,521.9	224.1	1992	3.69	25.4	7.67	2.28	42.22	13.53	36.77	1.12	7.43	9.73	

M = Mio-pliocene aquifer; S = Senonian aquifer.

Table 3: Field and analytical data for the Phreatic aquifer.

Locality	Site	Lat.	Long.	Elev.	Date	EC		T	pH	Alk.	Cl <sup>-</sup>	SO <sub>4</sub> <sup>2-</sup>	Na <sup>+</sup>	K <sup>+</sup>	Mg <sup>2+</sup>	Ca <sup>2+</sup>	Br <sup>-</sup>
						mS cm <sup>-1</sup>	°C										
				/m								/mmolL <sup>-1</sup>					
Khezama	P433	3,597,046	719,626	118	20/01/2013	2,09	22,7	9,18	1,56	12,02	7,3	13	0,99	4,34	2,8		
Khezama	P433	3,597,046	719,626	118	1992	2	22,1	8,86	1,46	12	6,87	11,57	0,93	4,4	2,9		
Hassi Mhould	R059	3,547,216	718,358	124	27/01/2013	2,1	23,9	8,15	1,86	13	7,3	11,57	1,25	4,43	3,43	0,024	
Ain Kheir	P106				1992	4,01	23,79	7,52	1,86	14,15	17,89	15,89	0,61	10,61	7,5		
Hassi Nagra	PLX3	3,584,761,4	717,604,5	125	20/01/2013	2,93	23	8,09	2,04	17,77	9,4	16,6	0,93	5,75		0,031	
	LTP 30				1992	4,08	23,73	7,12	5,25	18,21	9,97	24,29	0,41	1,43	8,13		
Maison de culture	PL31	3,537,988	720,114	124	1992	2,31	23,83	8,08	1,46	18,91	7,8	26,05	0,62	2,13			
El Bour	R006	3,544,272	719,421	161	1992	2,96	23,45	7,88	1,27	18,98	7,74	12,41	4,25	5,32	5,31		
Hassi Mhould	R059	3,547,216	718,358	124	1992	2,77	27,5	8,29	3,29	22,1	12,4	21,8	2,21	8,61	5,47		
Oglet Larba	P430	3,567,287,5	750,058,8	139	24/01/2013	4,5	23,45	7,83	4,22	20,83	9,366	34,17	2,69	1,35	0,86		
Maison de culture	PL31	3,537,988	720,114	124	28/01/2013	3,7	27,5	8,23	4,22	22,1	8,6	28,4	2,21	2,21	4,01		
France El Koum	P401	3,572,830,2	719,211,4	112	20/01/2013	3,44	27,5	7,52	2,21	23,3	13,4	21,8	2,21	1,86	8,25		
Gherbouz	PL15	3,537,962	718,744	134	1992	2,47	23,47	7,72	2,99	23,54	13,97	50,56	2,82	0,98	6,28		
Bour El Hachia	P408	3,544,999,3	719,930,6	110	1992	2,43	23,80	7,39	2,39	24,16	13,23	41,89	0,88	2,34	0,84		
Station d'epuration	PL30	3,538,398	721,404	130	20/01/2013	4,08	24,2	8,38	4,39	24,32	21,22	24,26	1,77	2,23	2,23	0,025	
France Ank Djemel	P422	3,575,339	724,063,3	127	1992	4,7	23,61	7,22	2,02	25,68	10,36	14,83	0,24	9,33	4,18		
Kouate Ain Bidia	PLX2	3,577,944,8	714,428,5	111	20/01/2013	4,1	25,2	7,39	3,01	24,16	13,23	21,22	2,32	4,96	7,46	0,033	
H Chegga	PLX4	3,547,329,7	716,520,7	129	27/01/2013	3,66	24,6	7,61	3,03	26,2	10,6	24	2,29	4,96	7,46	0,033	
Hassi Mhould	R058	3,548,943	717,253	133	1992	5,3	23,44	7,69	1,34	28,21	11,48	17,58	2,03	11,48	8,57		
Kouate Ain Mousssa	R057	3,533,586	714,060	141,6	1992	2,62	23,87	7,76	2,84	30,87	16,66	58,74	0,03	0,83	0,73		
Kouate El Gokla	PL15	3,537,109,4	718,419,1	137	1992	4,67	23,87	7,89	1,75	28,77	14,52	58,74	0,03	0,83	0,73		
Mekranah	PL18	3,537,270	721,119	119	31/01/2013	4,67	22,2	7,89	1,75	30,87	16,66	58,74	0,03	0,83	0,73		
Polyclinique Badobes	PL18	3,537,270	721,119	119	1992	4,49	23,67	7,58	1,5	31,2	15,4	21,3	2,05	11,17	8,57		
H Chegga	PLX4	3,577,944,8	714,428,5	111	1992	4,49	23,67	7,58	1,5	31,2	15,4	21,3	2,05	11,17	8,57		
Kouate El Gokla	PL16	3,532,463	713,715	117	1992	5,62	23,69	7,62	1,45	31,94	12,83	22,23	0,8	10,55	7,53		
Gherbouz	PL15	3,537,962	718,744	134	21/01/2013	4,65	23,3	8,16	1,78	32,4	14,6	20,05	0,8	10,83	7,89		
Kouate El Gokla	PL17	3,531,435	713,298	111	1992	4,77	23,70	7,70	1,55	32,81	12,85	22,23	0,8	10,55	7,53		
Kouate Ain Mousssa	R057	3,548,943	717,253	133	26/01/2013	5,7	26,2	7,64	1,96	33,6	12,1	29,2	3,35	5,98	5,98		
Ecole paramedicale	PL52	3,538,478	720,170	131	21/01/2013	5,72	22,9	8,21	1,96	33,6	12,1	29,2	3,35	5,98	5,98		
DSA	PL10	3,537,035	719,746	114	1992	6,08	23,71	7,69	1,32	35,01	13,52	37,1	1,92	19,37	8,17		
Kouate El Gokla	PL17	3,531,435	713,298	111	03/02/2013	5,5	25	7,72	1,52	35,4	13,8	37,1	1,92	19,37	8,17		
Kouate El Gokla	PL16	3,532,463	713,715	117	03/02/2013	5,8	22,5	8,04	1,66	36,3	11,6	38,4	3,21	3,21	5,68		
Station d'epuration	PL30	3,538,398	719,746	130	31/01/2013	5,29	25,1	7,84	1,66	36,3	11,6	38,4	3,21	3,21	5,68		
Hassi Debeh	P416	3,537,035	720,922	106	24/01/2013	5,5	24,6	8,86	2,37	38,6	18	28,5	4,45	6,75	8,37		
DSA	PL10	3,538,292,9	719,746	114	24/01/2013	5,51	24,6	8,44	2,37	38,6	18	28,5	4,45	6,75	8,37		
Hospital	LTPSN2	3,536,077	720,442,9	132	27/01/2013	6,09	24,5	7,78	1,62	39,7	11,7	36	0,89	9,03	9,03	2,126	
PARC SONNACOM	PL28	3,549,993	719,558	134	21/01/2013	6,08	24,5	8,13	1,82	39,8	11,8	30,6	1,17	5,11	5,97		
Bour El Hachia	P408	3,544,999,3	719,930,6	110	27/01/2013	6,22	23,1	8,07	1,82	42,14	10,72	18,87	1,86	13,59	8,46		
Kouate Ain Mousssa	R056	3,549,933	717,022	128	1992	7,62	23,65	7,93	0,36	42,5	19,1	18,87	1,86	13,59	8,46		
Kouate Ain Mousssa	R056	3,549,933	717,022	128	1992	7,62	23,65	7,93	0,36	42,5	19,1	18,87	1,86	13,59	8,46		
Ecole Oksa B. Nafaa	PL41	3,538,660	719,831	127	31/01/2013	6,36	24,1	7,68	2,11	44,9	13,2	36,2	1,18	12,49	8,07	6,32	

Table 4: Field and analytical data for the Phreatic aquifer (continued).

Locality	Site	Lat.	Long.	Elev.	Date	EC /mS.cm <sup>-1</sup>	T /°C	pH	Alk.	Cl <sup>-</sup>	SO <sub>4</sub> <sup>2-</sup>	Na <sup>+</sup> /mmol.L <sup>-1</sup>	K <sup>+</sup>	Mg <sup>2+</sup>	Ca <sup>2+</sup>
PARC HYDRAULIQUE	P419	3,539,494	725,605	132	31/01/2013	7,03	26,4	7,84	2,05	45,1	14,4	41,4	10,78	5,95	6,91
Parc hydraulique	PL13	3,536,550	720,200	123	21/01/2013	7,22	24,5	7,51	3,24	47,8	14,5	44,4	10,55	6,35	6,59
Mekhadma	P506	3,536,230	718,708	129	21/01/2013	7,64	27,1	7,94	1,78	48	14,6	42,9	6,56	7,4	7,61
Said Oba	P506	3,535,238,1	725,075,1	126	04/02/2013	8,32	24,3	8,12	1,71	52,6	17,58	33,32	10,97	7,51	7,83
Said Oba	P566	3,535,238,1	725,075,1	126	19/02	6,7	23,28	7,46	1,8	54,39	17,58	33,32	4,11	22,16	5,17
Mekhadma	PL17	3,540,433,1	719,661,3	115	27/01/2013	9	24,6	7,64	1,72	62,5	15,2	71,6	3,03	4,61	6,06
Mekhadma	PL13	3,536,908	718,511	130	21/01/2013	9,4	24,5	8,06	3,39	63,2	15,6	77,2	2,51	4,08	5,11
Mekhadma	PL13	3,530,116,2	722,775,1	130	04/02/2013	10,09	30,2	7,91	1,63	63,6	21,5	88,3	4,08	4,21	4,65
Mekhadma	PL25	3,536,230	718,708	129	19/02	9,5	23,72	7,96	0,63	75,57	10,62	10,22	2,64	32,94	9,54
Mekhadma (Bab-sha)	P066	3,542,636,5	718,957,4	126	19/02	7,75	23,48	7,62	1,51	80,23	12,45	45,87	2,46	23,59	5,91
CEM Malek B. Nabi	PL03	3,540,010,9	725,738,1	130	19/02	7,34	23,86	7,60	3,04	84,14	30,58	108,55	2,23	10,17	8,99
ENTV	PL21	3,536,074	721,268	128	19/02	9,73	23,82	7,25	4,46	84,26	23,68	61,62	3,75	33,53	1,88
Hôtel Transat	PL23	3,538,419	720,950	126	19/02	1,5	24,2	8,2	4,53	86,6	16,7	79,9	3,21	14,54	6,85
Mekhadma	PL21	3,536,074	721,268	128	28/01/2013	16,41	25,7	7,45	1,97	99,9	17,4	85,5	5,7	15,66	7,6
Mekhadma	PL05	3,537,109,4	718,419,1	137	21/01/2013	16,8	24,8	7,64	2,02	101,3	17,7	85,9	5,85	16,69	7,59
Beni Thour	PL44	3,537,675	721,673,9	134	19/02	4,68	23,85	7,19	2,74	109,75	67,21	134,67	5,71	42,02	8,77
Tazegrant	PLSNI	3,537,675	719,416	125	22/01/2013	17,08	24,9	8	3,41	114,2	18,1	92,9	12,8	16,85	7,81
CEM Malek B. Nabi	PL03	3,540,010,9	725,738,1	130	27/01/2013	10,84	23,1	7,54	3,29	117,3	14,7	116,4	2,06	8,99	7,24
El Bour	P006	3,564,272	719,421	161	03/02/2013	18,31	23,6	7,71	2,38	131,9	18,1	96,3	8,61	52,44	6,25
Ain Moussa	P015	3,551,711	720,591	103	19/02	12,42	26,4	7,85	4,03	138	16,7	108,8	13,06	19,51	7,99
Station de pompage	PL04	3,541,410,1	723,501,1	138	27/01/2013	19,01	26,4	7,67	2,68	142,22	24,5	125,9	3,1	27,11	8,72
Drain Chott Ouargla	D.Ch				19/02		23,88	7,8	4,96	153	17,7	96,31	3,16	44,22	3,02
Beni Thour	PL44	3,536,039,3	721,673,9	134	28/01/2013	20,18	25,8	7,8	4,96	153	17,7	96,31	3,16	44,22	3,02
Beni Thour	PL27	3,535,474	718,407	126	21/01/2013	21,23	24,8	8,11	1,7	169,4	18,4	130,3	6,29	22,83	8,08
CNMC	PL07	3,540,137	716,721	118	26/01/2013	22,31	27,2	7,57	4,33	171,5	17,1	130,8	6,32	28,01	8,83
Bameridil	P041	3,559,563	716,543	135	25/01/2013	25,94	24,5	8,18	7,95	208,6	13,4	198,9	3,61	11,81	8,75
N'Goussa	P009	3,559,388	717,707	123	26/01/2013	27,51	28,4	8,39	11,45	208,8	15,8	195,1	2,65	18,7	9,01
N'Goussa	LTP16				19/02	11,53	23,78	7,48	3,84	213,35	48,63	147,9	7,46	75,31	4,25
Chert Adjadja Aven	PLX1	3,540,758,8	726,115,6	132	28/01/2013	17,18	23,64	7,59	3,37	235,01	46,44	264,84	4,74	25,57	5,56
Route Frane	P003	3,569,043	721,496	134	02/02/2013	32,93	23,4	7,95	4,44	245,6	20,9	141,4	26,88	44,56	17,66
El Bour-N' gouca	PLX2	3,562,236	718,651	129	26/01/2013	31,03	23,5	8,01	6,91	252,7	17,9	208,2	9,41	29,99	10,03
Route Ain Bida	P015	3,537,323,9	724,063,3	127	21/01/2013	30,07	28,4	7,76	5,42	254,7	15,5	270,4	10,43	28,82	7,51
Ain Moussa	P015	3,551,711	720,591	103	25/01/2013	43,25	25,7	8,07	5,15	262,2	9,3	206,9	15,5	62,77	21,46
Ain Moussa	P402	3,549,503	721,514	138	25/01/2013	32,02	22,7	8,03	2,95	263	15,4	206,9	6,56	32,12	9,95
Route Frane	P001	3,572,148	722,366	127	19/02	60	28,7	8,6	7,69	313,2	93,9	442,8	23,26	12,56	10,17
Ain Moussa	P014	3,551,466	719,339	131	02/02/2013	60,58	23,63	8,37	4	323,62	58,13	331,43	5,01	49,77	3,97
Ain Moussa	P019	3,562,060	717,719	113	26/01/2013	61,06	23,40	7,31	3,98	336,96	64,29	328,67	5,53	62,37	5,45
N'Goussa	P018	3,562,122	716,590	110	25/01/2013	49,04	27,8	7,65	6,02	356,2	96	432,5	29,77	21,02	26,23
Ain Moussa	P014	3,551,466	719,339	131	25/01/2013	61,06	26,2	8,42	6,46	372,4	82,3	347,1	22,64	60,71	26,63
Route Sedrata	P113	3,535,586	714,576	105	03/02/2013	62,24	24,8	7,89	5,96	390,7	21,1	389,3	2,41	18,97	7,39
N'Goussa	P009	3,559,388	717,707	123	19/02	62,24	23,27	7,84	2,4	426,85	57,81	393,83	9,13	59,13	12,02

Table 5: Field and analytical data for the Phreatic aquifer (continued).

Locality	Site	Lat.	Long.	Elev.	Date	EC	T	pH	Alk.	Cl <sup>-</sup>	SO <sub>4</sub> <sup>2-</sup>	Na <sup>+</sup>	K <sup>+</sup>	Mg <sup>2+</sup>	Ca <sup>2+</sup>
			/m			/ms <sup>-1</sup>	/°C					/mmol/L			
Route Frane	P001	3,572,148	722,366	127	02/02/2013	66.16	28.3	7.24	6.49	468.7	101.5	350.3	25.96	116.21	35.31
Sekketi Safoume	P031	3,577,804	720,172	120	1992		23.75	7.31	6.32	481.83	43.35	326.82	12.61	94.15	23.56
Sekketi Safoume	P031	3,577,804	720,172	120	02/02/2013	75.96	27.9	8.06	5.85	500.3	110.3	470.5	28.67	79.12	35.47
Route Frane	P002	3,570,523	722,028	108	1992		23.81	7.76	6.29	522.39	182.95	653.78	9.97	104.7	10.59
Sekketi Safoume	P030	3,577,253	721,936	130	1992		23.52	7.72	4.43	527.7	123.48	533.79	11.59	106.21	10.65
Qum Karab	P012	3,554,089	718,612	114	25/01/2013	64.05	30.3	7.83	7.77	534.3	20.9	529.6	6.41	19.73	4.73
Qum Karab	P012	3,554,089	718,612	114	1992		23.41	7.46	2.72	539.55	60.64	413.55	5.55	112.77	9.42
ANK Djemel	P423	3,540,881	723,178	102	31/01/2013	90.8	23.5	7.48	6.19	645.07	101.3	495.5	5.89	125.81	30.32
Sekketi Safoume	P096	3,572,253	724,729	111	1992		23.59	7.71	3.69	650.7	78.46	357.28	15.97	208.4	12.86
Sekketi Safoume	P030	3,572,253	721,936	130	03/02/2013	100.1	31	7.83	3.71	671.8	90.3	742.9	10.71	41.46	7.65
N'Goussa	P017	3,560,256	715,781	105	26/01/2013		23.55	7.13	3.78	679.3	114.1	597.8	53.6	125.85	26.29
ANK Djemel	P021	3,573,943	723,161	105	1992		23.55	7.43	4.24	700.77	154.45	608.68	56.07	163.08	14.24
Sauton de pompage	PL04	3,541,410	723,501.1	138	1992		23.57	7.42	2.37	716.27	34.75	651.5	77.72	99.58	11.04
Route Frane	P002	3,570,523	722,028	108	02/02/2013	62.82	26.9	7.57	1.65	748.5	62.6	615.9	23.46	77.72	27.29
Sekketi Safoume	P096	3,540,265	724,729	110	03/02/2013	68.31	25.9	7.72	1.44	771	53.1	615.9	23.46	69.64	50.39
Sekketi Safoume	P096	3,540,265	724,729	110	1992		23.30	7.18	2.42	779.13	77.13	711.46	9.23	77.72	27.29
N'Goussa	P019	3,562,960	717,719	113	1992		23.30	7.72	2.37	788.5	62.6	615.9	23.46	69.64	50.39
Route Frane	P002	3,570,523	722,028	108	02/02/2013	62.82	26.9	7.57	1.65	748.5	62.6	615.9	23.46	77.72	27.29
Sekketi Safoume	P096	3,540,265	724,729	110	03/02/2013	68.31	25.9	7.72	1.44	771	53.1	615.9	23.46	69.64	50.39
Sekketi Safoume	P096	3,540,265	724,729	110	1992		23.30	7.18	2.42	779.13	77.13	711.46	9.23	77.72	27.29
N'Goussa	P019	3,562,960	717,719	113	1992		23.30	7.72	2.37	788.5	62.6	615.9	23.46	69.64	50.39
Route Frane	P002	3,570,523	722,028	108	02/02/2013	62.82	26.9	7.57	1.65	748.5	62.6	615.9	23.46	77.72	27.29
Sekketi Safoume	P096	3,540,265	724,729	110	03/02/2013	68.31	25.9	7.72	1.44	771	53.1	615.9	23.46	69.64	50.39
Sekketi Safoume	P096	3,540,265	724,729	110	1992		23.30	7.18	2.42	779.13	77.13	711.46	9.23	77.72	27.29
N'Goussa	P019	3,562,960	717,719	113	1992		23.30	7.72	2.37	788.5	62.6	615.9	23.46	69.64	50.39
Route Frane	P002	3,570,523	722,028	108	02/02/2013	62.82	26.9	7.57	1.65	748.5	62.6	615.9	23.46	77.72	27.29
Sekketi Safoume	P096	3,540,265	724,729	110	03/02/2013	68.31	25.9	7.72	1.44	771	53.1	615.9	23.46	69.64	50.39
Sekketi Safoume	P096	3,540,265	724,729	110	1992		23.30	7.18	2.42	779.13	77.13	711.46	9.23	77.72	27.29
N'Goussa	P019	3,562,960	717,719	113	1992		23.30	7.72	2.37	788.5	62.6	615.9	23.46	69.64	50.39
Route Frane	P002	3,570,523	722,028	108	02/02/2013	62.82	26.9	7.57	1.65	748.5	62.6	615.9	23.46	77.72	27.29
Sekketi Safoume	P096	3,540,265	724,729	110	03/02/2013	68.31	25.9	7.72	1.44	771	53.1	615.9	23.46	69.64	50.39
Sekketi Safoume	P096	3,540,265	724,729	110	1992		23.30	7.18	2.42	779.13	77.13	711.46	9.23	77.72	27.29
N'Goussa	P019	3,562,960	717,719	113	1992		23.30	7.72	2.37	788.5	62.6	615.9	23.46	69.64	50.39
Route Frane	P002	3,570,523	722,028	108	02/02/2013	62.82	26.9	7.57	1.65	748.5	62.6	615.9	23.46	77.72	27.29
Sekketi Safoume	P096	3,540,265	724,729	110	03/02/2013	68.31	25.9	7.72	1.44	771	53.1	615.9	23.46	69.64	50.39
Sekketi Safoume	P096	3,540,265	724,729	110	1992		23.30	7.18	2.42	779.13	77.13	711.46	9.23	77.72	27.29
N'Goussa	P019	3,562,960	717,719	113	1992		23.30	7.72	2.37	788.5	62.6	615.9	23.46	69.64	50.39
Route Frane	P002	3,570,523	722,028	108	02/02/2013	62.82	26.9	7.57	1.65	748.5	62.6	615.9	23.46	77.72	27.29
Sekketi Safoume	P096	3,540,265	724,729	110	03/02/2013	68.31	25.9	7.72	1.44	771	53.1	615.9	23.46	69.64	50.39
Sekketi Safoume	P096	3,540,265	724,729	110	1992		23.30	7.18	2.42	779.13	77.13	711.46	9.23	77.72	27.29
N'Goussa	P019	3,562,960	717,719	113	1992		23.30	7.72	2.37	788.5	62.6	615.9	23.46	69.64	50.39
Route Frane	P002	3,570,523	722,028	108	02/02/2013	62.82	26.9	7.57	1.65	748.5	62.6	615.9	23.46	77.72	27.29
Sekketi Safoume	P096	3,540,265	724,729	110	03/02/2013	68.31	25.9	7.72	1.44	771	53.1	615.9	23.46	69.64	50.39
Sekketi Safoume	P096	3,540,265	724,729	110	1992		23.30	7.18	2.42	779.13	77.13	711.46	9.23	77.72	27.29
N'Goussa	P019	3,562,960	717,719	113	1992		23.30	7.72	2.37	788.5	62.6	615.9	23.46	69.64	50.39
Route Frane	P002	3,570,523	722,028	108	02/02/2013	62.82	26.9	7.57	1.65	748.5	62.6	615.9	23.46	77.72	27.29
Sekketi Safoume	P096	3,540,265	724,729	110	03/02/2013	68.31	25.9	7.72	1.44	771	53.1	615.9	23.46	69.64	50.39
Sekketi Safoume	P096	3,540,265	724,729	110	1992		23.30	7.18	2.42	779.13	77.13	711.46	9.23	77.72	27.29
N'Goussa	P019	3,562,960	717,719	113	1992		23.30	7.72	2.37	788.5	62.6	615.9	23.46	69.64	50.39
Route Frane	P002	3,570,523	722,028	108	02/02/2013	62.82	26.9	7.57	1.65	748.5	62.6	615.9	23.46	77.72	27.29
Sekketi Safoume	P096	3,540,265	724,729	110	03/02/2013	68.31	25.9	7.72	1.44	771	53.1	615.9	23.46	69.64	50.39
Sekketi Safoume	P096	3,540,265	724,729	110	1992		23.30	7.18	2.42	779.13	77.13	711.46	9.23	77.72	27.29
N'Goussa	P019	3,562,960	717,719	113	1992		23.30	7.72	2.37	788.5	62.6	615.9	23.46	69.64	50.39
Route Frane	P002	3,570,523	722,028	108	02/02/2013	62.82	26.9	7.57	1.65	748.5	62.6	615.9	23.46	77.72	27.29
Sekketi Safoume	P096	3,540,265	724,729	110	03/02/2013	68.31	25.9	7.72	1.44	771	53.1	615.9	23.46	69.64	50.39
Sekketi Safoume	P096	3,540,265	724,729	110	1992		23.30	7.18	2.42	779.13	77.13	711.46	9.23	77.72	27.29
N'Goussa	P019	3,562,960	717,719	113	1992		23.30	7.72	2.37	788.5	62.6	615.9	23.46	69.64	50.39
Route Frane	P002	3,570,523	722,028	108	02/02/2013	62.82	26.9	7.57	1.65	748.5	62.6	615.9	23.46	77.72	27.29
Sekketi Safoume	P096	3,540,265	724,729	110	03/02/2013	68.31	25.9	7.72	1.44	771	53.1	615.9	23.46	69.64	50.39
Sekketi Safoume	P096	3,540,265	724,729	110	1992		23.30	7.18	2.42	779.13	77.13	711.46	9.23	77.72	27.29
N'Goussa	P019	3,562,960	717,719	113	1992		23.30	7.72	2.37	788.5	62.6	615.9	23.46	69.64	50.39
Route Frane	P002	3,570,523	722,028	108	02/02/2013	62.82	26.9	7.57	1.65	748.5	62.6	615.9	23.46	77.72	27.29
Sekketi Safoume	P096	3,540,265	724,729	110	03/02/2013	68.31	25.9	7.72	1.44	771	53.1	615.9	23.46	69.64	50.39
Sekketi Safoume	P096	3,540,265	724,729	110	1992		23.30	7.18	2.42	779.13	77.13	711.46	9.23	77.72	27.29
N'Goussa	P019	3,562,960	717,719	113	1992		23.30	7.72	2.37	788.5	62.6	615.9	23.46	69.64	50.39
Route Frane	P002	3,570,523	722,028	108	02/02/2013	62.82	26.9	7.57	1.65	748.5	62.6	615.9	23.46	77.72	27.29
Sekketi Safoume	P096	3,540,265	724,729	110	03/02/2013	68.31	25.9	7.72	1.						

Table 6: Isotopic data  $^{18}\text{O}$  and  $^3\text{H}$  and chloride concentration in Continental Intercalaire, Complexe Terminal and Phreatic aquifers (sampling campaign in 1992).

Phreatic aquifer											
Piezometer	$\text{Cl}^-$ /mmol L $^{-1}$	$\delta^{18}\text{O}$ /‰	$^3\text{H}$ /UT	Piezometer	$\text{Cl}^-$ /mmol L $^{-1}$	$\delta^{18}\text{O}$ /‰	$^3\text{H}$ /UT	Piezometer	$\text{Cl}^-$ /mmol L $^{-1}$	$\delta^{18}\text{O}$ /‰	$^3\text{H}$ /UT
P007	1.860.5	-2.49	0	PL15	23.54	-7.85	0.6(1)	P074	4.356.4	3.42	6.8(8)
P009	426.85	-6.6	1.2(3)	P066	80.23	-8.14	0.8(1)	PL06	14.15	-8.13	1.0(2)
P506	54.39	-6.83	1.6(3)	PL23	1,103.32	-6.1	0	PL30	24.32	-7.48	2.4(4)
P018	818.67	-2.95	6.2(11)	P063	1,379.3	-3.4	8.7(15)	P002	522.39	-5.71	0.6(1)
P019	779.13	-4.67	5.6(9)	P068	2,335.6	-3.04	8.8(14)	PL21	84.26	-7.65	1.2(2)
PZ12	2,405.5	-2.31	8.1(13)	P030	527.7	-6.57	2.4(4)	PL31	18.91	-7.38	1.6(3)
P023	1,176.9	-2.62	0.2(1)	P076	1,743.5	-5.56	2.8(5)	P433	12	-8.84	0
P416	2,433.7	-7.88	5.9(9)	P021	700.7	-5.16	2.6(4)	PL03	84.14	-7.35	1.7(3)
P034	2,752	-1.77	5.7(9)	PL04	716.27	-2.89		PL44	109.75	-8.82	1.0(2)
P036	4,972.7	3.33	2.1(4)	P093	2,198.5	-2.64	5.1(8)	PL05	30.87	-7.44	1.9(3)
P037	4,953.8	3.12	1.8(3)	P096	645.07	-6.13	4.8(8)	P408	24.16	-7.92	0
P039	4,189.5	0.97	2.2(4)	PLX1	1,296.6	-5.6	1.1(2)	P116	31.94	-7.18	1.1(2)
P041	2,599.7	-0.58	7.3(13)	PLX2	25.68	-7.6	1.3(2)	LTP 16	213.35	-7.48	1.6(3)
P044	2,106.1	-4.46	2.7(5)	P015	134.68	-6.77	3.0(5)	P117	32.81	-6.92	0.1
P014	336.96	-6.9	2.8(5)	P001	323.62	-4.66	2.5(4)	PL10	35.01	-7.31	0.2(1)
P012	539.3	-6.41	2.2(4)	P100	235.01	-5.81	0	PL25	75.57	-7.41	0.9(2)
P042	2,330.8	2.05	6.0(10)	P056	42.14	-7.03	2.9(5)	LTP30	18.21	-7.5	1.1(2)
P006	18.98	-6.64	0.5(1)	P113	954.89	-4.75	0.8(2)	LTP06	1,638.6	-1.97	2.8(5)
P057	28.21	-7.33	1.1(2)	PLX4	31.52	-7.1	0.3(1)	P031	481.83	-6.06	3.0(5)
P059	20.83	-7.81	0	P115	28.77	-2.54	6.8(12)				

Complexe Terminal aquifer											
Borehole	$\text{Cl}^-$ /mmol L $^{-1}$	$\delta^{18}\text{O}$ /‰	$^3\text{H}$ /UT	Borehole	$\text{Cl}^-$ /mmol L $^{-1}$	$\delta^{18}\text{O}$ /‰	$^3\text{H}$ /UT	Borehole	$\text{Cl}^-$ /mmol L $^{-1}$	$\delta^{18}\text{O}$ /‰	$^3\text{H}$ /UT
D5F80	42.22	-7.85		D1F138	28.92	-8.13	0.7(1)	D2F71	13.53	-8.23	0.6(1)
D3F8	29.81	-8.14	1.4(2)	D3F18	21.66	-8.23	0.2(1)	D7F4	10.6	-8.27	0.1(1)
D3F26	34.68	-7.97	0.8(1)	D3F10	14.27	-7.88	1.5(2)	D2F66	11.02	-8.3	
D4F94	20.05	-8.18	0.6(1)	D6F51	28.39	-7.9	0.7(1)	D1F151	10.75	-8.32	0.4(1)
D6F67	18.79	-8.23	3.7(6)	D1F135	18.08	-7.97	1.1(2)	D6F64	11.36	-8.28	4.3(7)

Continental Intercalaire aquifer											
Borehole	$\text{Cl}^-$ /mmol L $^{-1}$	$\delta^{18}\text{O}$ /‰	$^3\text{H}$ /UT	Borehole	$\text{Cl}^-$ /mmol L $^{-1}$	$\delta^{18}\text{O}$ /‰	$^3\text{H}$ /UT	Borehole	$\text{Cl}^-$ /mmol L $^{-1}$	$\delta^{18}\text{O}$ /‰	$^3\text{H}$ /UT
Hadeb I	5.8	-8.02	0	Hadeb II	6.19	-7.93	0.1(1)	Aouinet Moussa	6.49	-7.88	1.1(2)

Table 7: Statistical parameters for Continental Intercalaire (CI), Complexe Terminal (CT) and Phreatic (Phr) aquifers samples selected on the basis of  $\delta^{18}\text{O}$  and  $\text{Cl}^-$  data (see text).

Aquifer	Size	Parameter	EC /mS cm $^{-1}$	T /°C	pH	Alk.	$\text{Cl}^-$	$\text{SO}_4^{2-}$	$\text{Na}^+$	$\text{K}^+$	$\text{Mg}^{2+}$	$\text{Ca}^{2+}$
							/mmol/L					
CI	11	Average	2.2	49.0	7.5	2.3	11.0	4.7	10.3	0.51	3.6	2.4
CI	11	Stdd. dev.	0.3	2.0	0.2	1.0	4.6	2.5	4.6	0.23	2.0	1.8
CT	50	Average	3.2	23.0	7.8	2.3	20.0	8.9	17.0	1.0	5.5	5.6
CT	50	Stdd. dev.	1.1	2.4	0.4	0.8	7.0	2.6	6.0	0.8	2.2	1.7
Phr cluster I	30	Average	3.9	24.0	7.9	2.3	24.7	11.8	24.2	2.1	7.2	5.3
Phr cluster I	30	Stdd. dev.	1.3	1.3	0.4	1.0	6.9	3.4	11.0	1.7	5.0	2.7
Phr cluster II	3	Average		23.4	7.0	2.4	4,761.0	158.0	4,021.0	32.4	500.0	13.0
Phr cluster II	3	Stdd. dev.		0.1	0.5	1.6	350.0	43.0	1,093.0	28.0	378.0	8.0

Table 8: Summary of mass transfer for geochemical inverse modeling. Phases and thermodynamic database are from Phreeqc 3.0 (Parkhurst and Appelo, 2013).

Phases	Stoichiometry	CI/CT	CT/Phr I	Rainwater/P036	PhrI/PhrII 60%/40%
Calcite	CaCO <sub>3</sub>	—	$-6.62 \times 10^{-6}$	$-1.88 \times 10^{-1}$	$-2.26 \times 10^{-1}$
CO <sub>2</sub> (g)	CO <sub>2</sub>	$-6.88 \times 10^{-5}$	—	$8.42 \times 10^{-4}$	$5.77 \times 10^{-4}$
Gypsum	CaSO <sub>4</sub> · 2 H <sub>2</sub> O	$4.33 \times 10^{-3}$	—	$1.55 \times 10^{-1}$	$1.67 \times 10^{-1}$
Halite	NaCl	$7.05 \times 10^{-3}$	$3.76 \times 10^{-3}$	6.72	1.28
Sylvite	KCl	$2.18 \times 10^{-3}$	$1.08 \times 10^{-3}$	$4.02 \times 10^{-1}$	—
Bloedite	Na <sub>2</sub> Mg(SO <sub>4</sub> ) <sub>2</sub> · 4 H <sub>2</sub> O	—	$1.44 \times 10^{-3}$	—	—
Huntite	CaMg <sub>3</sub> (CO <sub>3</sub> ) <sub>4</sub>	—	—	$4.74 \times 10^{-2}$	$5.65 \times 10^{-2}$
Ca ion exchange	CaX <sub>2</sub>	$-1.11 \times 10^{-3}$	—	—	—
Mg ion exchange	MgX <sub>2</sub>	$1.96 \times 10^{-3}$	—	$1.75 \times 10^{-1}$	$-2.02 \times 10^{-1}$
Na ion exchange	NaX	—	—	—	$3.92 \times 10^{-1}$
K ion exchange	KX	$-1.69 \times 10^{-3}$	—	$-3.49 \times 10^{-1}$	$1.20 \times 10^{-2}$

Values are in mol/kg (H<sub>2</sub>O). Positive (mass entering solution) and negative (mass leaving solution) phase mole transfers indicate dissolution and precipitation, respectively; — indicates no mass transfer.



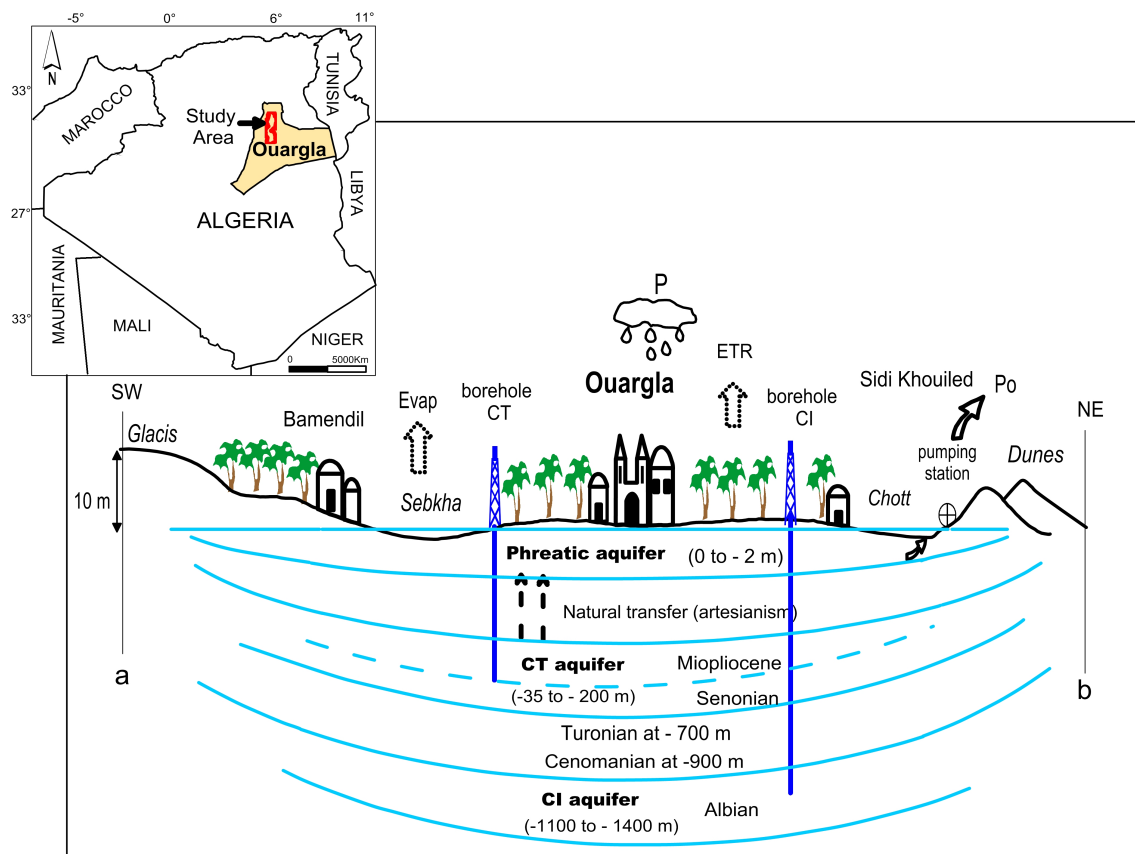


Figure 1: Localisation and schematic relations of aquifers in Ouargla. *Blue lines represent limits between aquifers, and the names of aquifers are given in bold letters; as the limit between Senonian and Mio-pliocene aquifers is not well defined, a dashed blue line is used. Names of villages and cities are given in roman (Bamendil, Ouargla, Sidi Khouiled), while geological/geomorphological features are in italic (Glacis, Sebkh, Chott, Dunes). Depths are relative to the ground surface. Letters a and b refer to the cross section (fig. 2) and to the localisation map (fig. 3).*

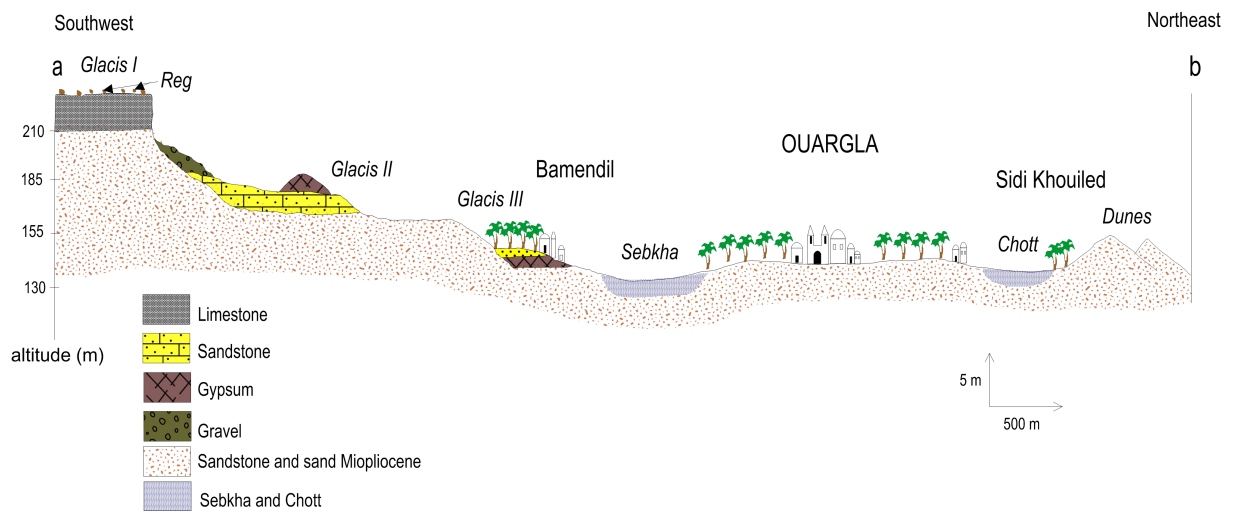


Figure 2: Geologic cross section in the region of Ouargla.  
*The blue pattern used for Chott and Sebkha correspond to the limit of the saturated zone.*

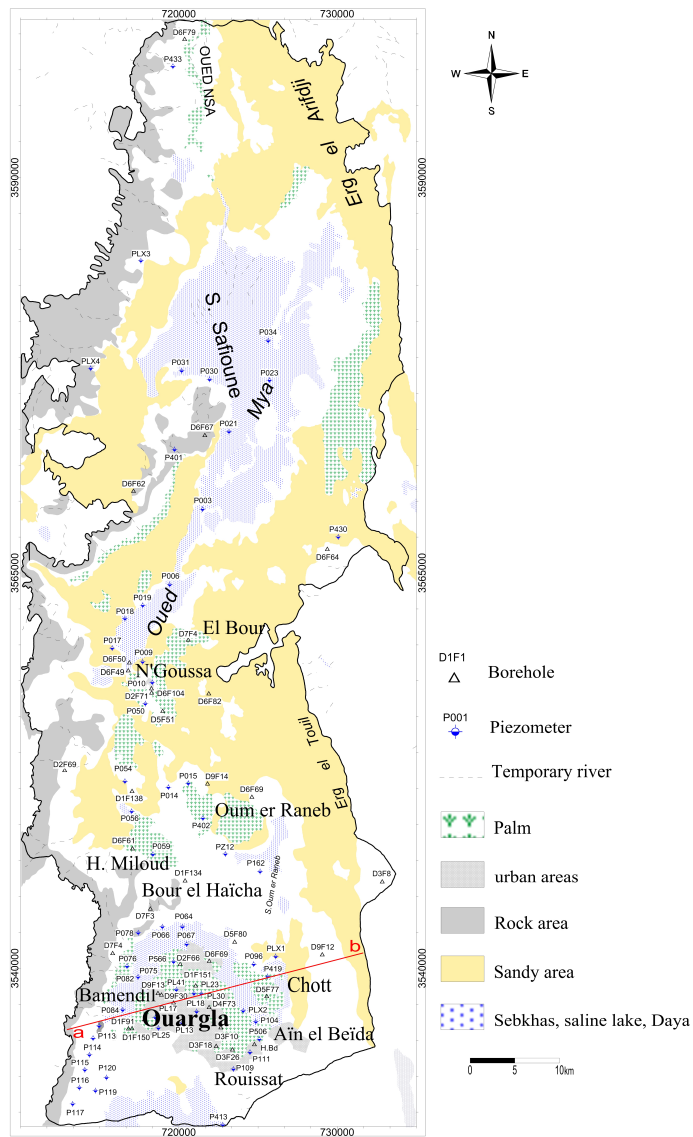


Figure 3: Localisation map of sampling point

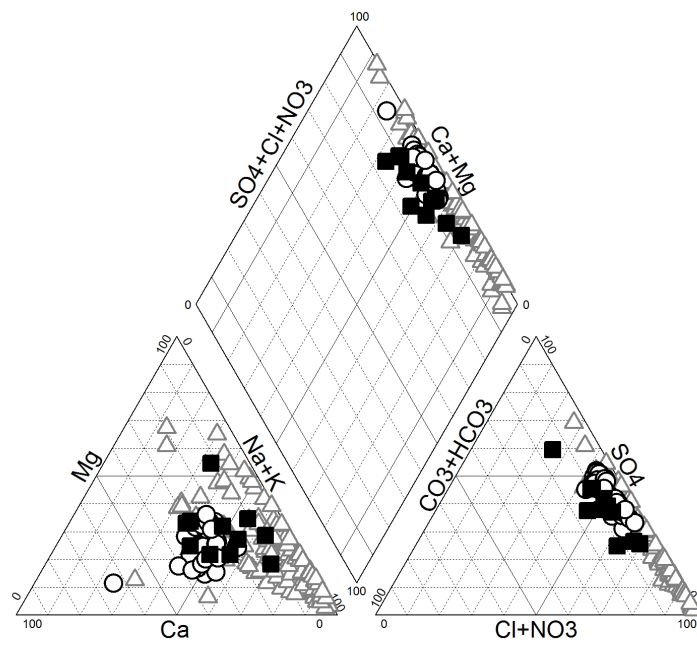
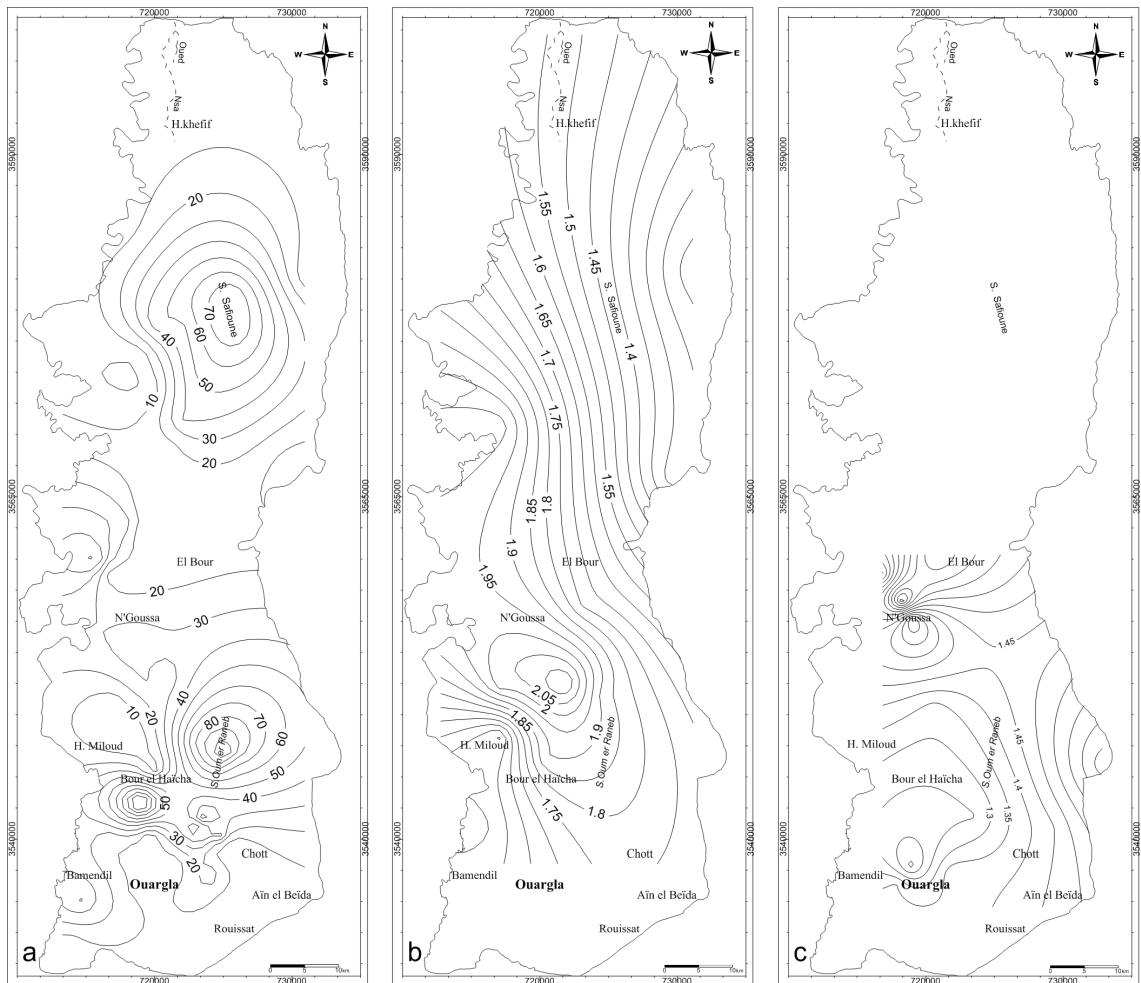


Figure 4: Piper diagram for Continental Intercalaire (filled squares), Complexe Terminal (open circles) and Phreatic aquifer (open triangles).



5

Figure 5: Contour maps of the salinity (expressed as global mineralization) in the aquifer system, (a) Phreatic aquifer; (b) and (c) Complex Terminal [(b) Mio-pliocene and (c) Senonian]; figures are isovalues of global mineralization (values in g/L).

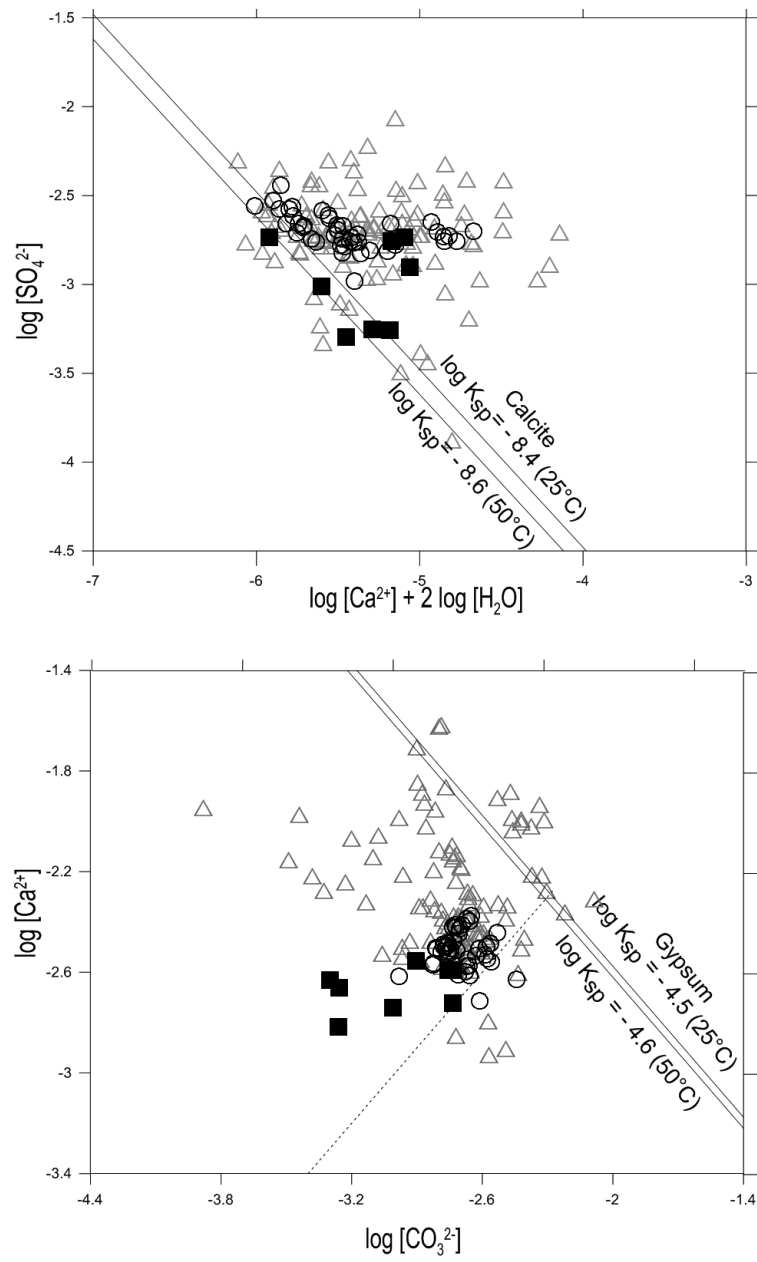


Figure 6: Equilibrium diagrams of calcite (top) and gypsum (bottom) for Continental Intercalaire (filled squares), Complexe Terminal (open circles) and Phreatic aquifer (open triangles). Equilibrium lines are defined as:  $\log[\text{Ca}^{2+}] + \log[\text{CO}_3^{2-}] = \log K_{sp}$  for calcite, and  $\log[\text{Ca}^{2+}] + 2 \log[\text{H}_2\text{O}] + \log[\text{SO}_4^{2-}] = \log K_{sp}$  for gypsum.

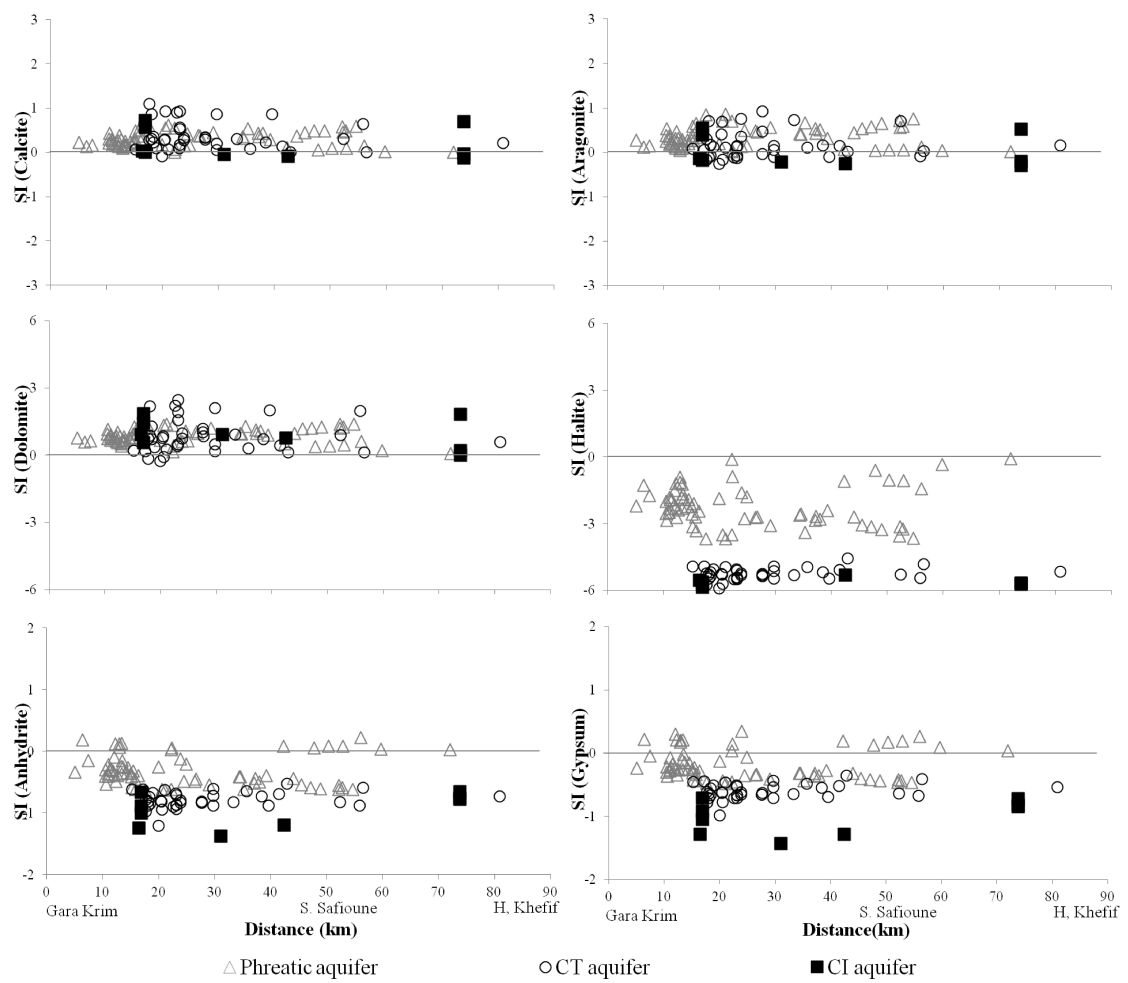


Figure 7: Variation of saturation indices with distance from south to north in the region of Ouargla.

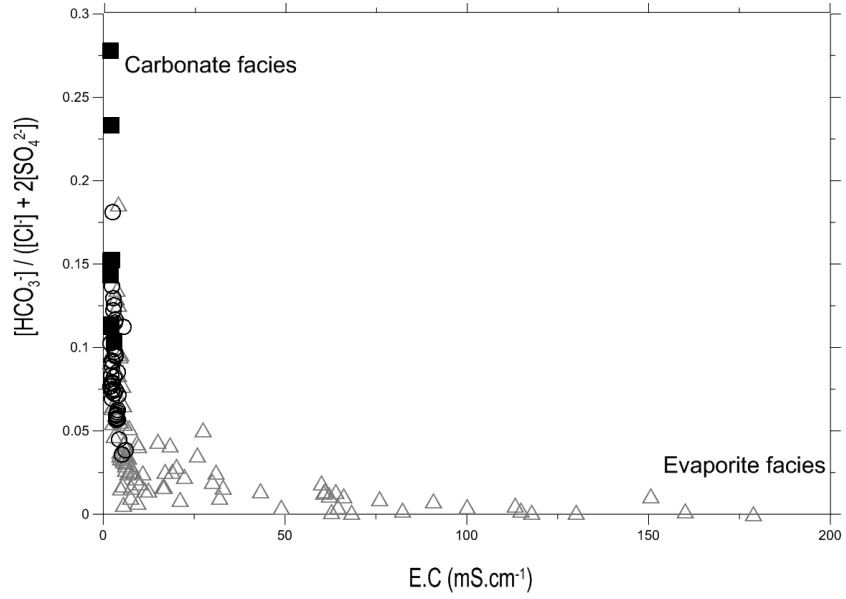


Figure 8: Change from carbonate facies to evaporite from Continental Intercalaire (filled squares), Complexe Terminal (open circles) and Phreatic aquifer (open triangles).

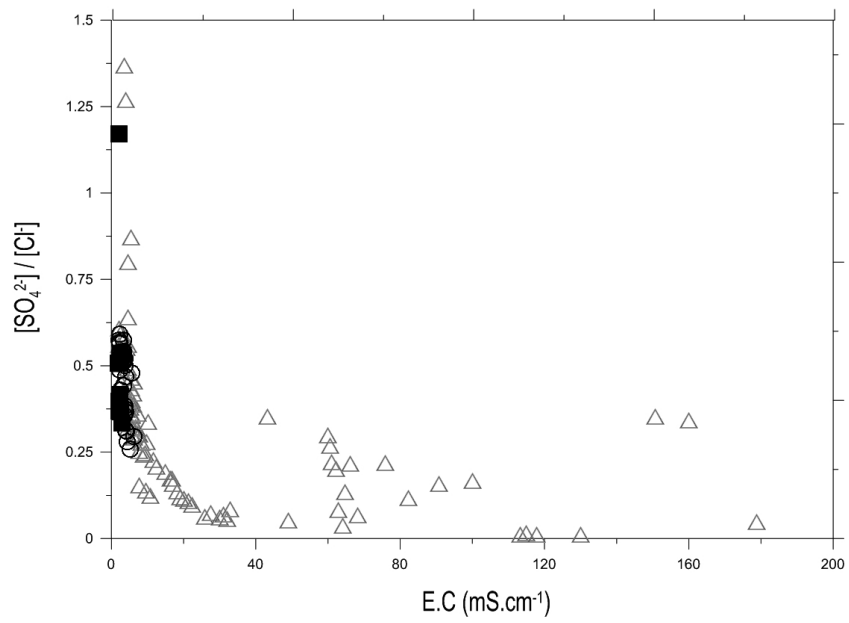


Figure 9: Change from sulfate facies to chloride from Continental Intercalaire (filled squares), Complexe Terminal (open circles) and Phreatic aquifer (open triangles).



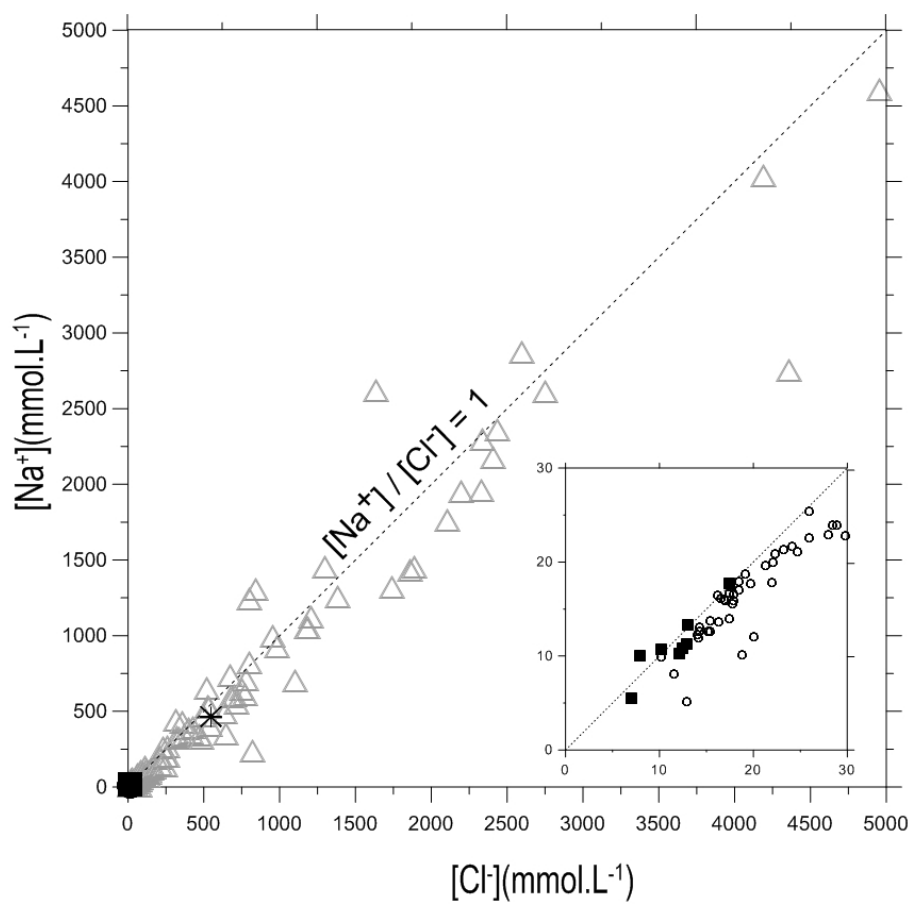


Figure 10: Correlation between  $\text{Na}^+$  and  $\text{Cl}^-$  concentrations in Continental Intercalaire (filled squares), Complexe Terminal (open circles) and Phreatic aquifer (open triangles). Seawater composition (star) is  $[\text{Na}^+] = 459.3 \text{ mmol L}^{-1}$  and  $[\text{Cl}^-] = 535.3 \text{ mmol L}^{-1}$  (Stumm and Morgan, 1999, p.899).

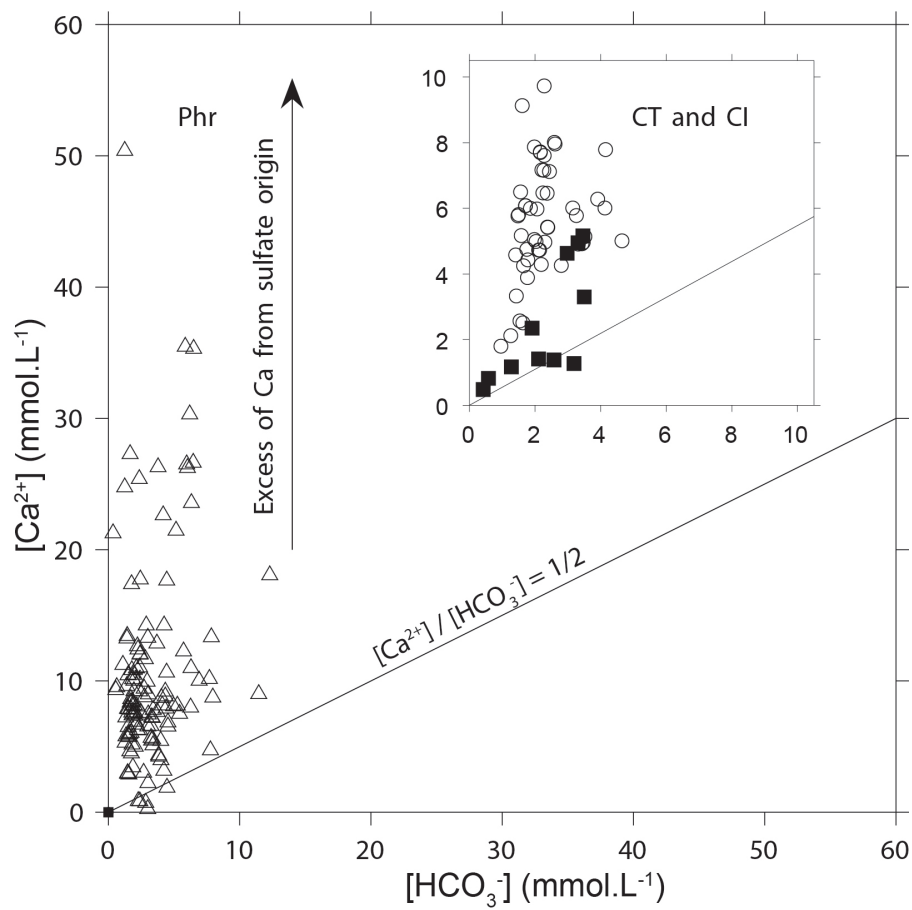


Figure 11: Calcium vs.  $HCO_3^-$  diagram in Continental Intercalaire (filled squares), Complexe Terminal (open circles), Phreatic aquifer (open triangles) and Seawater composition (star) is  $[Ca^{2+}] = 10.2 \text{ mmol.L}^{-1}$  and  $[HCO_3^-] = 2.38 \text{ mmol.L}^{-1}$  (Stumm and Morgan, 1999, p.899).

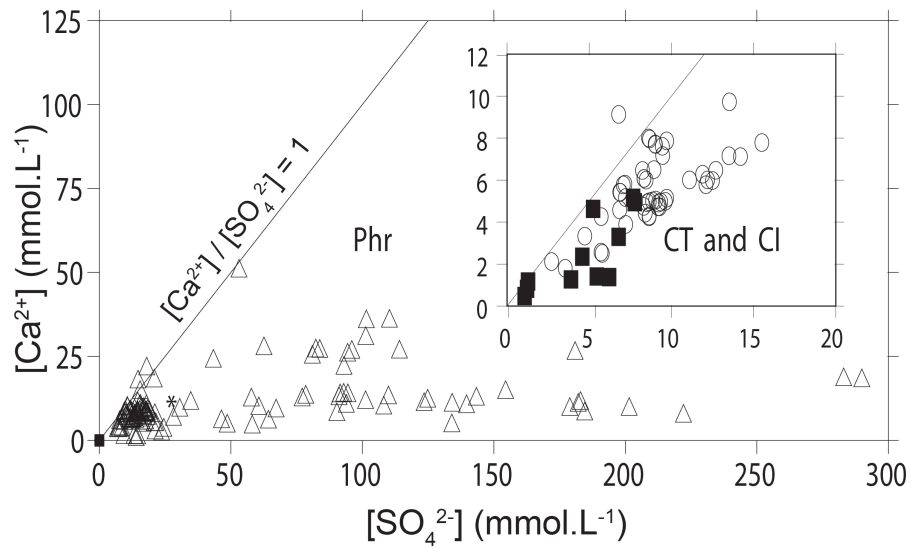


Figure 12: Calcium vs.  $\text{SO}_4^{2-}$  diagram in Continental Intercalaire (filled squares), Complexe Terminal (open circles), Phreatic aquifer (open triangles) and Seawater composition (star) is  $[\text{Ca}^{2+}] = 10.2 \text{ mmol L}^{-1}$  and  $[\text{SO}_4^{2-}] = 28.2 \text{ mmol L}^{-1}$  (Stumm and Morgan, 1999, p.899).

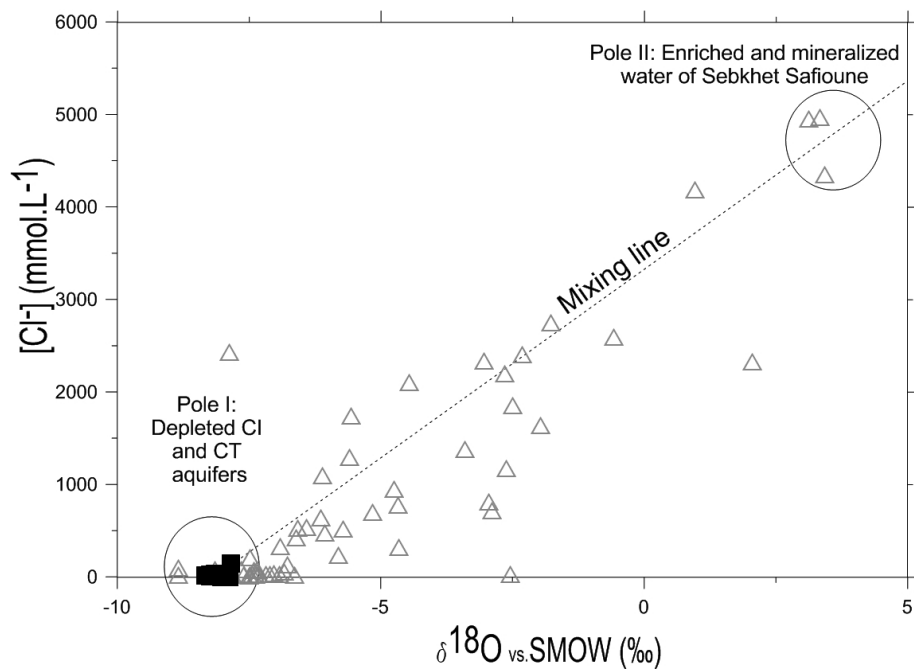


Figure 13: Chloride concentration versus  $\delta^{18}\text{O}$  in Continental Intercalaire (filled squares), Complexe Terminal (open circles) and Phreatic aquifer (open triangles) from Ouargla.

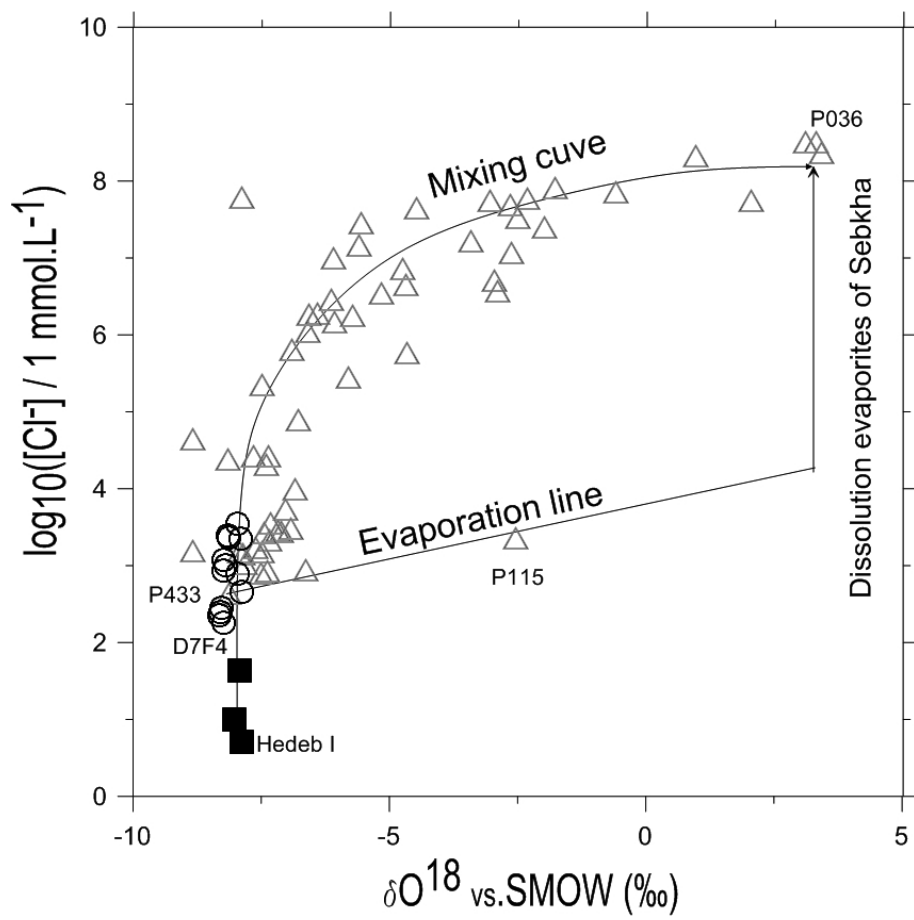


Figure 14: Log  $[\text{Cl}^-]$  concentration versus  $\delta^{18}\text{O}$  in Continental Intercalaire (filled squares), Complexe Terminal (open circles) and Phreatic aquifer (open triangles) from Ouargla.